Variations in the Malvinas Current volume transport since October 1992

Aurélie Spadone[1] and Christine Provost[1]

Received 22 April 2008; revised 22 October 2008; accepted 14 November 2008; published 6 February 2009.

[1] We present a set of new current meter measurements collected to monitor the Malvinas Current (MC) near its merger with the Brazil Current at 40–41°S from December 2001 to February 2003 below a Jason-1 altimeter track. These measurements are compared to former measurements obtained 8 years earlier at the same location; they also provide new information on the core of the MC on the continental slope above the 1000-m isobath where a mooring had been previously lost. There, most of the velocity variation is along-isobath (80% of the variance) and shows a significant annual cycle. The two data sets provide coherent means and statistical parameters on the vertical structure of the flow. A 14-year-long time series of MC volume transport is derived using satellite altimetry. The good correlation between the altimetry-derived transport and the transport estimated from the current meter data persists in time (over 0.7 for each measurement period). A spectacular shift in the spectral composition of transport variations was observed: from 1992 until the end of 1997 transport variations occurred at rather short periods (50–90 days and to some degree around 180 days) whereas, after year 2000, longer periods including a seasonal cycle predominated. Altimetry-derived anomalies of surface geostrophic velocities along the core of the MC show a similar shift in spectral composition suggesting a remote-forcing origin.

Citation: Spadone, A., and C. Provost (2009), Variations in the Malvinas Current volume transport since October 1992, *J. Geophys. Res.*, *114*, C02002, doi:10.1029/2008JC004882.

1. Introduction

[2] The Malvinas Current (MC) is part of the northern branch of the Antarctic Circumpolar Current (ACC) [*Piola and Gordon*, 1989] that carries the cold (<7°C at the surface in winter) and relatively fresh sub-Antarctic water equatorward along the western edge of the Argentine Basin (Figure 1). It follows the 1000–1500 m isobaths along the Patagonian shelf break, until it meets the Brazil Current at the latitude (38°S) of the Rio de La Plata estuary. After they meet, both currents separate from the coast and turn offshore. The MC retroflects cyclonically southward, whereas the Brazil Current separates into two branches, one branch turning northward forming a recirculation cell, while the other branch flows southward and returns to the northeast at about 45°S [*Peterson and Stramma*, 1991]. The latter branch is referred to as the overshoot of the Brazil Current. The meeting of the MC and the Brazil Current is known as the Brazil-Malvinas Confluence. It is one of the most energetic regions of the world ocean [*Provost and LeTraon*, 1993]. The strong contrasts in the surface waters of the Confluence make satellite imagery particularly useful for examining surface variability on a wide range of temporal and spatial scales [e.g., *Olson et al.*, 1988; *Provost et al.*, 1992; *Vigan et al.*, 2000; *Saraceno et al.*, 2004, 2005; *Barré et al.*, 2006]. Inverted echosounders and altimetry have been used to monitor the location of the Confluence and the baroclinic transport of the Brazil Current [e.g., *Garzoli and Garraffo*, 1989; *Garzoli*, 1993; *Goni et al.*, 1996; *Goni and Wainer*, 2001]. Ocean models, whether analytical [e.g., *Agra and Nof*, 1993; *Lebedev and Nof*, 1997] or forced ocean general circulation models [e.g., *Matano*, 1993; *Matano et al.*, 1993; *Smith et al.*, 1994], showed the importance of the relative strength of the Brazil Current and MC transports in determining variations in the Confluence.

[3] The first current-velocity time series data on the MC were collected from December 1993 to June 1995, at 41°S [*Vivier and Provost*, 1999a, hereinafter referred to as VP99a], near the confluence with the Brazil Current (Figure 1), as part of the World Ocean Circulation Experiment (WOCE). These measurements showed that the mean flow of the MC is equivalent-barotropic in form (for a definition, see *Killworth* [1992]), whereas the variability is dominated by a surface-intensified barotropic-like mode, the structure of which is suggestive of mode coupling due to the steep topography. This mode appeared to become progressively more exactly barotropic with decreasing depth. Owing to the premature failure of a mooring, a reliable volume transport time series could only be calculated for 254 days, with a mean transport of about 41.5 Sv (Sv = 10^6 m^3 s^{-1}). Transport variations were found to have a standard deviation of 12.2 Sv, a significant part of which was due to the mesoscale activity at the Confluence, reducing to about half

[1]LOCEAN, UMR7159, MNHN, IRD, Université Pierre et Marie Curie, CNRS, Paris, France.

0148-0227/09/2008JC004882

of this for timescales beyond 2 months. The barotropic component of the flow accounted for about half of the total transport. The minimum and maximum transport values were almost one order of magnitude different and bracketed all reported estimated values in the literature (e.g., 10 Sv, by *Gordon and Greengrove* [1986]; 70 Sv, by *Peterson* [1992]; 60 Sv, by *Saunders and King* [1995]; 45 Sv, by *Maamaatuaiahutapu et al.* [1998]). The mean transport of the MC was comparable with that of the BC (e.g., 30 to 56 Sv, by *Maamaatuaiahutapu et al.* [1998]), suggesting that the momentum imparted by the MC was certainly responsible for the occurrence of the Brazil Current's mean separation from the coast at a latitude $\sim 10^\circ$ north of the climatological zero wind stress curl line, as discussed by *Matano* [1993], *Agra and Nof* [1993], or *Smith et al.* [1994].

[4] The ability of TOPEX/Poseidon altimeter data from ground track 26 (Figure 1) to monitor the MC transport was tested against in situ measurements [*Vivier and Provost*, 1999b, hereinafter referred to as VP99b]. The transport estimated from altimetric data was well correlated (0.8), with estimates based on the current meter data showing that the TOPEX/Poseidon altimeter could be used to sensitively monitor the flow in the upper 1500 m when its data are combined with the statistical information on the vertical structure of the current provided by the current meter measurements. A 5-year-long volume transport time series was derived (October 1992 to October 1997) and made it possible to study intraseasonal variability [*Vivier et al.*, 2001, hereinafter referred to as VPM]. Two main broad spectral peaks were identified in the MC variations: one at about 70 days and another at about 180 days. Comparatively little energy was found with an annual periodicity. Variability with a periodicity of about 70 days was coherent with bottom-pressure variability on the northern side of Drake Passage (lag less than 20 days) and was identified as a baroclinic shelf wave propagating along the edge of the Patagonian Plateau at a speed of 2.5 to 3 m s^{-1} (VPM). The second broad spectral peak in the MC transport, near the semiannual period, appeared to reflect a barotropic adjustment to changes in the wind stress curl north of 50°S, mostly in the Pacific sector (less than 20-day lag), suggesting that a time-varying Sverdrup balance was the most influential process in the MC transport. This was in contrast to the Antarctic Circumpolar Current, which is rather more sensitive to the zonally integrated wind stress [e.g., *Tansley and Marshall*, 2001, and references therein]. The marginal energy at the annual period in the MC transport suggested that the observed seasonal migration of the Confluence along the coast was not due to the MC transport variations, but was rather either due to the local wind stress curl [*Garzoli and Giulivi*, 1994] or imparted by fluctuations in the mass transport of the Brazil Current, which has a robust annual cycle in phase with the local wind stress curl [e.g., *Matano et al.*, 1993; *Goni and Wainer*, 2001]. However, variations in the MC transport are nonnegligeable relative to its mean transport ($\sim$25%) and may be important for the variations of the Confluence at other timescales (semiannual or interannual).

[5] Although, substantial variability in the location of the Confluence at interannual timescales has been reported [e.g., *Olson et al.*, 1988], its dynamics remain uncertain. Little is known about interannual variations in the Brazil Current baroclinic transport [e.g., *Goni and Wainer*, 2001]. Interannual variations in the MC transport were not examined by VPM, since the mean field was estimated with a too short an in situ time series. In order to examine the low-frequency variations of the MC transport, it is necessary to estimate again the mean flow over a period of a year or more, to compare it and combine it with the previous estimate. It is also necessary to determine whether the good agreement between the transport derived from in situ data and the transport derived from altimetric data for the 1993–1995 data set persists in time.

[6] For that purpose, within the Climate Variability and Prediction program (CLIVAR), an array of current meter moorings was deployed in 2001 across the MC at the same location as the first array but 8 years later (Figure 1). The new data and subsequent analyses are presented here.

[7] The paper is organized as follows. The data are presented in section 2. Basic statistics from the new current meter measurements in 2002–2003 are discussed and compared to those from the previous observations (section 3). A 14-year-long MC transport time series (1992–2007) is derived and analyzed in section 4. Results are summarized and discussed in section 5.

2. Data

2.1. Current Meter Data

[8] Three current meter moorings (M1, M2, and M3) were deployed below the Jason-1 track 26 in December 2001 and recovered in February 2003 from the Argentinean R/V *Puerto Deseado* (Figure 1). This minimal array was anchored across the MC, at 40°–41°S, at the same location as the first set (20 current meters on five moorings between December 1993 and June 1995). Each mooring carried two vector-averaging current meters (VACM), one at about 200 dbars and the second at a greater depth (500 dbars for M1, 700 dbars for M2, and 950 dbars for M3) (Figure 1 and Table 1). This minimal configuration resulted from the analysis of the data from the 1993–1995 moorings. M1 and M2 were placed so as to be in the current core, M1 being particularly important, since the mooring at this location in the former array was lost. M2 is important too; VP99b showed that the velocity from the shallow current meter at M2 and the MC total transport were highly correlated. M3 was located so as to document the MC's eastern boundary and should therefore be sometimes inside the MC and sometimes outside it, thus allowing an estimation of the MC's width. VP99b showed that 90% of the MC volume transport occurred in the upper 1500 m. They also showed that the vertical shear did not vary much; therefore two current meters on each mooring line were thought to be sufficient to estimate shear variations.

[9] A current meter is labeled Ci,j where i is the mooring number (i = 1, 2, 3) and j is the depth (j = 1, 2). Unfortunately, C3,1 failed prematurely (after 179 days), whereas the other current meters recorded for over 400 days (Table 1). The VACMs were calibrated for velocity and pressure, before and after deployment, at the Institut Français de Recherche pour l'Exploitation de la Mer (Ifremer). The reported velocity accuracies ranged between 1 and 2 cm s^{-1} for the various VACMs, with the minimum measurable current speeds ranging between 0.53 and 3.78 cm s^{-1}. The

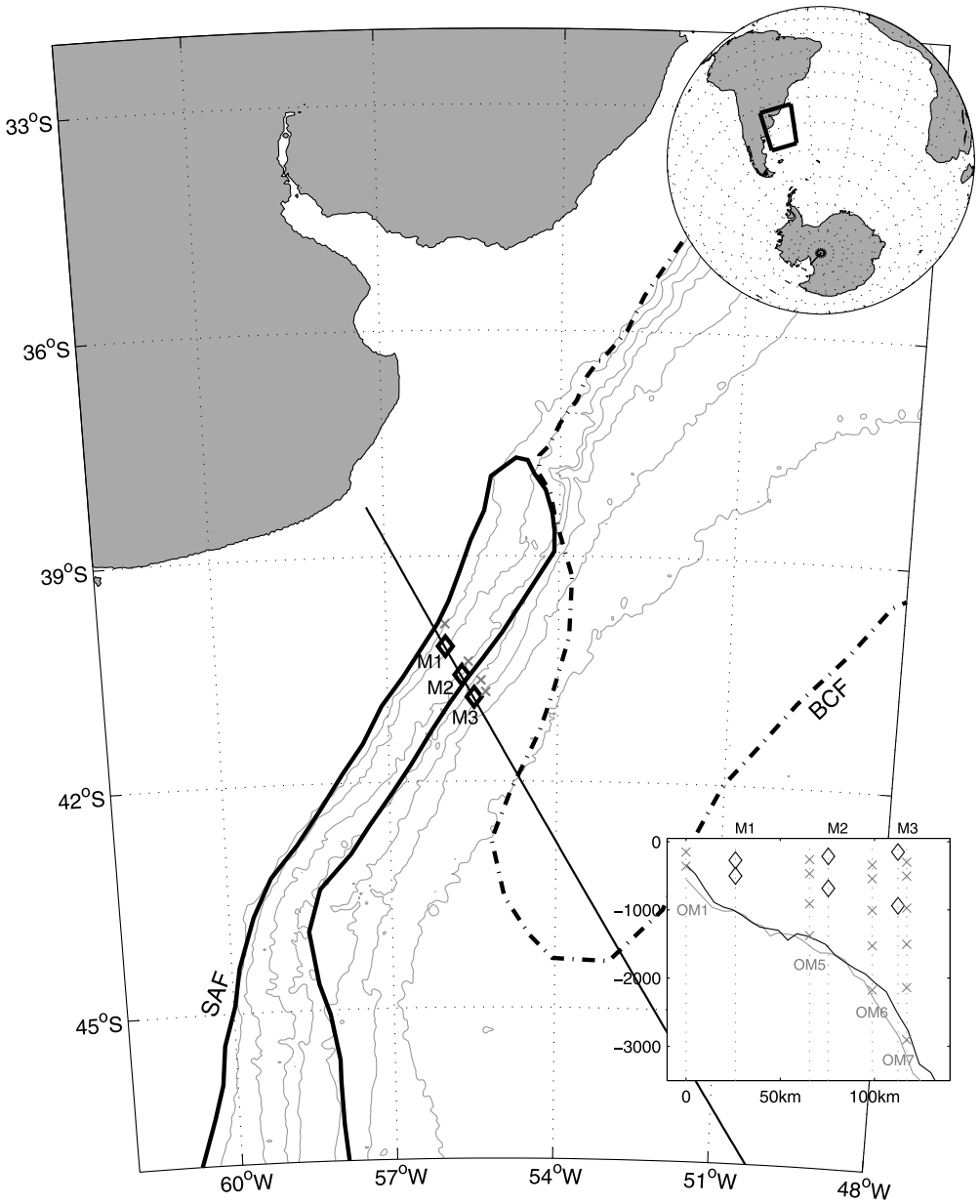

Figure 1. Location of the current meter moorings: a cross marks the location of the moorings deployed in 1993–1995 and a diamond marks the site of the moorings from 2001 to 2003. Jason track 26 (formerly TOPEX/Poseidon) is drawn in black. Bottom topography is from ETOPO-2 [500- 1000- 1500- 2000- 3000- 4000- 5000-m isobaths]. Mean location of the Subantarctic Front (SAF) (solid line) and Brazil Current Front (BCF) (dashed line) are from *Saraceno et al.* [2004] and mark the respective mean boundaries of the Malvinas Current and the Brazil Current. Inset to the bottom right: vertical distribution of the instruments along mooring lines: OM1 to OM7 are the moorings deployed in 1993–1995, (gray cross), M1 to M3 the moorings deployed in 2001–2003 (diamond).

reader is referred to the data report [*Kartavtseff*, 2005] for further details concerning technical information on the instruments, data calibration, and magnetic corrections.

[10] Moorings were pulled up and down severely during strong current pulses over periods of several days. The standard deviation of the vertical displacement was 30–60 m for the upper instruments (Table 1). Largest displacements occurred at moorings M3. They exceeded 150 m on two occasions, lasting a few days at C3,2 (nominal depth 940 m). The first event, around 10 May 2002, corresponded to a displacement of 250 m at C3,1 (nominal depth 150 m). The second event lasted from 20 to 25 September 2002 after C3,1 had stopped recording. At mooring M2, displacements exceeded 150 m at C2,1 (nominal depth 220 m) during three events occurring between 23 November and 10 December 2002, and during one of them the displacement reached up to 230 m. These events are described further in section 3. Errors on the velocity measurements due to these motions were discussed by VP99a (Appendix A). As the instruments are not sufficiently densely sampled on the vertical axis to

t1.1 **Table 1.** Statistical Parameters of Current Meter Measurements[a]

t1.2		M1 (1010 m)				M2 (1510 m)				M3 (2536 m)			
t1.3		C_{11} Aanderaa 4034		C_{12} Aanderaa 4259		C_{21} Aanderaa 11864		C_{22} Aanderaa 5813		C_{31} Aanderaa 5716		C_{32} Aanderaa 11729	
t1.4	Longitude	−55.9783				−55.6788				−55.4750			
t1.5	Latitude	−40.2020				−40.5823				−40.8770			
t1.6	Days	416		433		433		426		179		433	
t1.7	P (dbars)	274	*33*	502	*18*	217	*44*	685	*28*	153	*62*	942	*51*
t1.8	T (°C)	4.3	*0.2*	3.8	*0.2*	3.7	*0.3*	2.8	*0.1*	3.9	*0.5*	2.6	*0.1*
t1.9	*VU* (cm s^{-1})	18.6	*7.0*	20.4	*7.3*	19.5	*6.8*	19.8	*6.1*	8.9	*10.1*	10.3	*6.7*
t1.10	*VV* (cm s^{-1})	31	*11.8*	33.7	*12.4*	22.2	*6.5*	23.1	*7.1*	7.3	*11.9*	7.2	*6.8*

[a] C_{ij} denotes current meter j (from the surface) at mooring M_i. Bottom depth is indicated in brackets. Mean and standard deviation (italics). P is pressure, T is in situ temperature. VU is the eastward component and VV is the northward component of the daily averaged velocities (after 50-h low-pass filtering).
t1.11 $V_\perp$ is the velocity component orthogonal to the section.

guarantee accurate corrections, the velocity data are used as they are and the corresponding statistics refer to the mean depth of the instruments. In accordance with VP99a, we expected the mean velocity to be slightly biased (underestimated by 2%) and velocity variance to be underestimated by up to 20%.

[11] In the following sections, the velocity components and temperature data from the current meters have been low-pass-filtered, with a cutoff period of 50 h (in order to remove inertial and tidal variance) and then subsampled at a daily rate. Velocity components parallel and perpendicular to the isobath direction are shown on Figure 2.

2.2. Altimetric Data

[12] Satellite altimetric data provide a homogeneous time series since October 1992, from TOPEX/Poseidon from October 1992 to August 2002 and from Jason-1 thereafter. We used two types of altimetric products: maps of sea level anomaly (MSLA) to examine the mesoscale field, and the sea level anomaly data along track 26, to compute an MC volume-transport time series. Both altimeter products were produced by Ssalto/Duacs (Multimission ground segment: altimetry, orbitography and location/data unification, and altimetry combination system) and distributed by Archiving, Validation, and Interpretation of Satellite Oceanographic data (AVISO, http://www.aviso.oceanobs.com/). The MSLA have a 1/3-degree spatial resolution and a 7-day temporal resolution. The along track data $\eta(x, t)$ have a repeat period of 9.916 days and a spatial sampling about 6 km. To compute MC transport across track 26, we used the method developed by VP99b. The velocity V along the track at a distance x from the 300-m isobath, at depth z and at time t is expressed as:

$$\mathrm{V}(\mathrm{x},\mathrm{z},\mathrm{t}) = \mathrm{V}_m(\mathrm{x},\mathrm{z}) + \mathrm{A}(\mathrm{x},\mathrm{z})\mathrm{V}'(\mathrm{x},0,\mathrm{t}) \quad (1)$$

where $V_m(x, z)$ is a mean velocity field, A(x, z) is a function reflecting the vertical structure of the current, and $V'(x, 0, t)$ is the cross-track surface geostrophic velocity anomaly (SGVA). The SGVA V' is computed as:

$$\mathrm{V}' = -\mathrm{g}/\mathrm{f}\cdot(\partial\eta/\partial\mathrm{x}) \quad (2)$$

where g is the gravitational acceleration, f is the Coriolis parameter, η is the sea level anomaly (SLA), and x is the along-track coordinate. The mean velocity field $V_m(x, z)$ is built up taking into account both data sets of subsurface current meter measurements and information from surface drifters. The function reflecting the vertical structure of the current A(x, z) is the correlation coefficient between the cross-sectional velocities of the uppermost current meters and those of the underlying instruments, the correlation coefficient being normalized to unity at the surface, as in VP99b.

2.3. Surface Velocities From Drifters

[13] Satellite-tracked drifters collect data on upper ocean currents and sea surface temperatures (SST) globally under the IOC-WMO Drifting Buoy Programme, an operational ocean-observing network of surface drifters that return data on, inter alia, ocean near surface currents via the ARGOS satellite system. Drifter positions are estimated from 16 to 20 satellite fixes per day per drifter. The Drifter Data Assembly Center (DAC) at the Atlantic Oceanographic and Meteorological Laboratory (AOML), in Miami, assembles these raw data, applies quality control procedures, and interpolates them to 6-h intervals (http://www.aoml.noaa.gov/envids/gld/). The time series include position (latitude and longitude), velocity (zonal and meridional), temperature, time and wind velocity (zonal and meridional). The wind velocity data are obtained by interpolation of the National Center for Environmental Prediction (NCEP)'s wind reanalysis results for 10-m height at 6-hourly intervals at the drifter location. We use the data from the 64 drogued drifters that crossed the 40.1°–41.3°S and 55.1°–56.15°W area within the period 1994–2006 to estimate mean surface velocities (and their standard deviations) along the section, to contribute to the estimation of $V_m(x, z)$ for $z = 0$.

[14] The drifter velocity can be decomposed into an Ekman component, a geostrophic component, a residual ageostrophic component, and a slippage due to the wind, as follows:

$$\mathrm{U_d}(\mathrm{t}) = \mathrm{U_e}(\mathrm{t}) + \mathrm{U_{geo}}(\mathrm{t}) + \mathrm{U_{ageo}}(\mathrm{t}) + \mathrm{U_{slip}}(\mathrm{t}) \quad (3)$$

where $U_d(t)$ is the velocity measured from the drifter, $U_e(t)$ is the Ekman component, $U_{geo}(t)$ is the geostrophic component, $U_{ageo}(t)$ is the ageostrophic component, and U_{slip} is the slippage velocity due to the wind. The latter was quantified by *Niiler and Paduan* [1995] to be limited to 1 cm s^{-1} in 10 m s^{-1} wind at 10 m height for a drogued drifter. The Ekman component was calculated for each 6-hourly interval position along each drifter track using the wind stress computed from the 10-m NCEP wind reanalysis, as described by *Brambilla and Talley* [2006].

[15] Boxes of 0.2° latitude by 0.3° longitude were defined along the mooring array. Velocity means and variances were computed over the six boxes spanning the MC between the

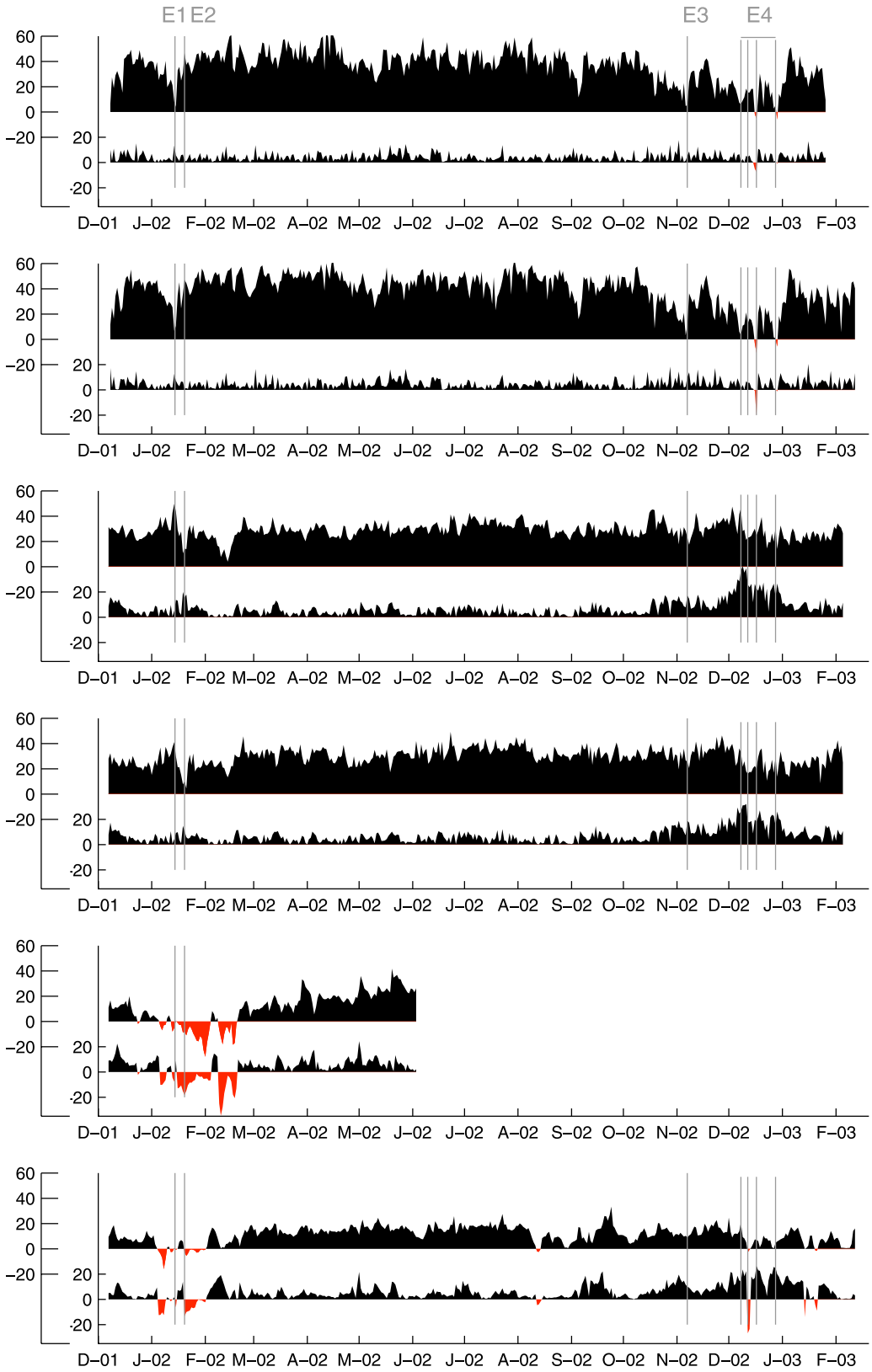

Figure 2. Time series of the along-isobath (first y axis) and cross-isobath (second y axis) velocity components; from top to bottom: C11, C12, C21, C22, C31, and C32. Units are cm s^{-1}. Negative velocity components are indicated in red. E1 to E4 corresponds to mesoscale events described in the text (section 3).

t2.1 **Table 2.** Statistical Parameters of Surface Drifter Data

t2.2 Box Latitude Range	Box Longitude Range	Isobath Range (m)	Number of Drifters (Total 64)	Mean Surface Cross Section Velocity (cm s^{-1})	Velocity Standard Deviation (cm s^{-1})
t2.3 40.1–40.3°S	56.15–55.85°W	600–1100	7	38.3	5.0
t2.4 40.3–40.5°S	56–55.7°W	1100–1350	14	45.7	4.2
t2.5 40.5–40.7°S	55.85–55.55°W	1350–1800	20	37.0	5.7
t2.6 40.7–40.9°S	55.7–55.4°W	1800–2600	11	22.5	5.6
t2.7 40.9–41.1°S	55.55–55.25°W	2600–3800	4	11.3	4.5
t2.8 41.1–41.3°S	55.4–55.1°W	3800–4400	8	−9.8	6.8

600-m and the 4400-m isobaths (Table 2). There is no seasonal bias in the distribution of the data in any of the six boxes. The number of drifters and the average and standard deviation of the cross-sectional velocity (which comprises both the geostrophic and ageostrophic components) for each box are reported in Table 2.

2.4. Ancillary Data: Satellite Imagery

[16] Sea surface temperature and ocean color images were used to infer a more global description of the currents and to discuss special events affecting the velocity records. Cloud detection is a problem in the interpretation of satellite imagery in the region [e.g., *Vigan et al.*, 2000; *Saraceno et al.*, 2004]. Exceptionally clear situations can be examined with instantaneous high-resolution images, as given in Figure 3. However, most of the time we had to make use of lower-resolution weekly composite images to be able to get to the ocean surface (Figure 4). Figure 3 illustrates a typical configuration of the southwest Atlantic in winter, with high temperatures (>16°C) associated with the Brazil Current and low temperatures (<7°C), with the Malvinas Current. Both currents have low surface chlorophyll-*a* (chl-*a*) concentrations (<0.2 mg m^{-3}). A continuous band of high chl-*a* values (>2 mg m^{-3}) along the shelf break is associated to the Patagonian shelf break front that separates the shelf waters from the colder waters of the MC [*Saraceno et al.*, 2005]. The La Plata River plume appears as an area of extremely high chl-*a* concentrations (>8 mg m^{-3}) that are probably overestimated because of the presence of terrigenous material and colored dissolved organic matter. The confluence of the currents is marked by a local maximum in the chl-*a* concentration due to advection from the shelf by the currents associated with the Brazil-Malvinas (B/M) front [*Barré et al.*, 2006]. *Saraceno et al.* [2004, 2005] showed that the B/M front pivots seasonally around a fixed point at approximately 39.5°S, 53.5°W, changing its orientation from N-S in winter to NW-SE in summer. Consequently, on average, the front

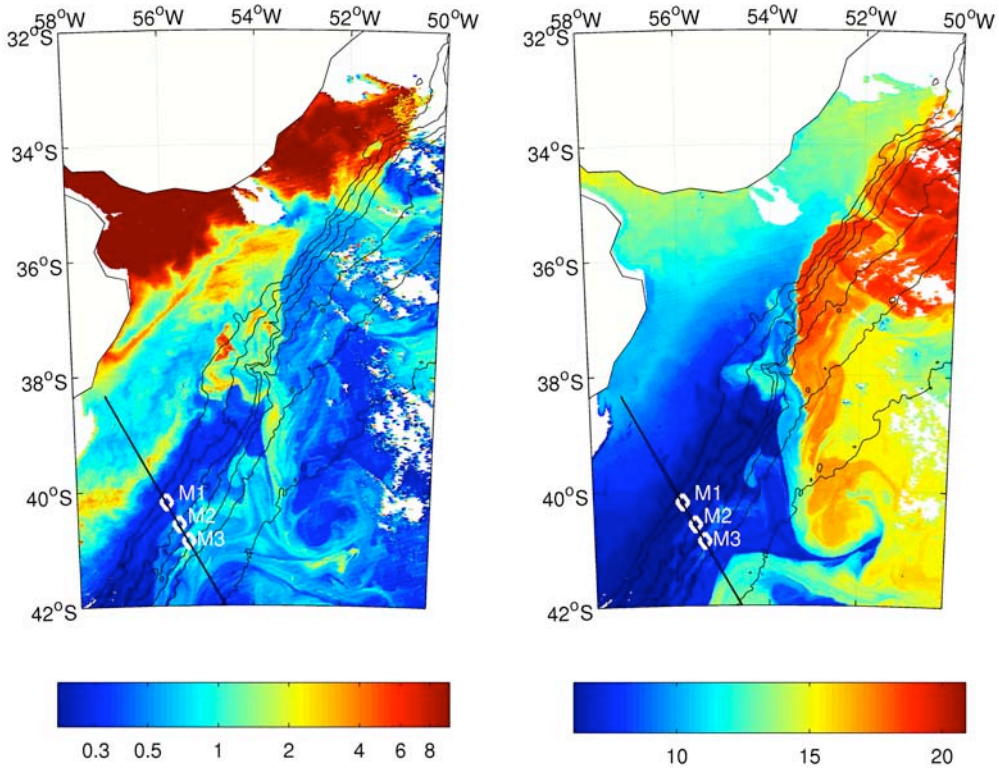

Figure 3. (right) Sea surface temperature and (left) chlorophyll-*a* concentration derived from 1.1-km resolution MODIS images on 22 August, 2002. Jason track 26 (formerly TOPEX/Poseidon) is drawn in black. Mooring locations are indicated by white dots. Bottom topography isolines mark the 500-, 1000-, 1500-, 2000-, 3000-, 4000-, and 5000-m isobaths. Units are mg/m^3 for chl-*a* and °C for SST.

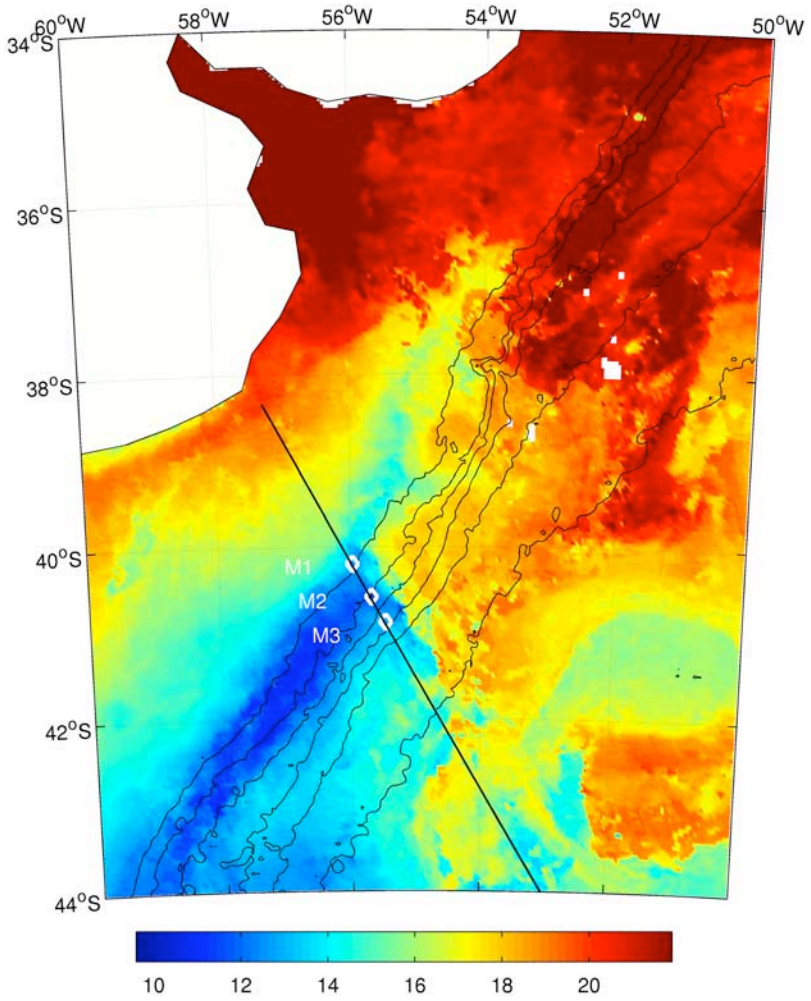

Figure 4. An 8-day composite image of sea-surface temperature image from 11 to 18 December 2002 (austral summer) with a 4-km pixel resolution from MODIS Aqua. It corresponds to event 4. The B/M front is very close to the mooring array. Bottom topography isolines mark the 500-, 1000-, 1500-, 2000-, 3000-, 4000-, and 5000-m isobaths. Temperature units are in °C.

intersects the 1000-m isobath at 38°30′S in summer and north of 37°S in winter.

3. Current Meter Observations in 2001–2003

3.1. Current Meter Observations in 2001–2003 and Description of the Currents From Satellite Imagery

[17] As planned, moorings M1 and M2 were within the MC core and mooring M3 was near the eastern limit of the current (Figure 2). Indeed, the current meters on moorings M1 and M2 provided a strong along-isobath velocity component (mean above 30 cm s^{-1}) and a small cross-isobath component (between 4 and 7 cm s^{-1}), whereas M3 current meters recorded more variable velocities (Table 1). From mid-December 2001 until mid-October 2002, that is, during the first 10 months of the record, the current was stronger at M1 than at M2 with a mean of about 45 cm s^{-1} and maximum velocities in excess of 60 cm s^{-1} at C1,1, whereas mean velocities and maxima at C2,1 hardly reached 30 and 50 cm s^{-1}, respectively (Table 1). The images from August 2002 (Figure 3) are typical of the long period (from 15 February to 10 October) during which the MC was strong and wide, the three moorings are within the MC, as suggested by C3,2 velocities, and the flow is stronger at M1 than at M2 (Figure 2). From mid-October to the end of December 2002 along-isobath velocities were weaker at M1 (mean about 18 cm s^{-1}) and stronger at M2 (mean about 30 cm s^{-1}) suggesting a more offshore location for the core of the MC.

[18] Although strong along-isobath velocities were the predominant feature at M1 and M2, on a few occasions the cross-isobath velocity component was larger than the along-isobath velocity component. These events with significant cross-isobath velocity components are labeled 1 to 4 in Figure 2. The most conspicuous of them (labeled 4 in Figure 2) occurred in December 2002, with a strong cross-isobath flow at M2 and a weak and sometimes even reversed flow at M1, which lasted about a month. It corresponded to a situation in which the B/M front is at a particularly southern location (Figure 4), extremely close to the mooring array. Velocity amplitudes of 60 cm s^{-1} and 40 cm s^{-1} were recorded at C2,1 and C2,2, probably associated with currents of the B/M front. The other events with significant cross-isobath velocities were of short

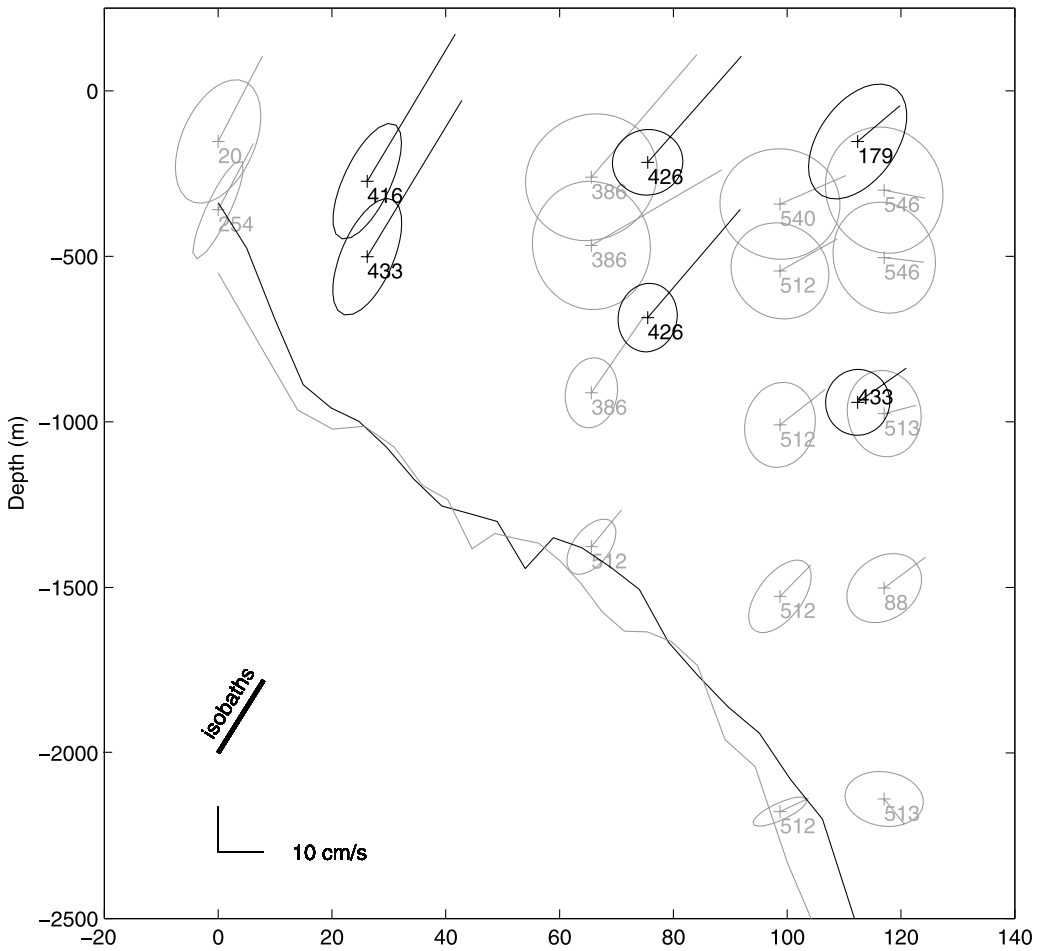

Figure 5. Mean flow and variance ellipses for each current meter along the section: in gray from the WOCE time series (1993–1995), in black from the 2001–2003 time series. The mean direction of isobaths is indicated by the thick solid line at bottom left. Number of data days is indicated on the right-hand side of the ellipses. The bottom topography of the two sections (moorings M1 to M3 deployed in 2001–2003 and moorings OM1 to OM7 deployed in 1993–1995) is indicated by the black and gray lines, respectively; x axis is distance along the section in kilometers, the origin being the OM1 location.

duration (a few days) and corresponded to two different situations. Event 1 (14 January 2002) was characterized by a weakening of the along-isobath component and an increase in the cross-isobath component at M1. It was accompanied by a simultaneous increase in the along-isobath component at M2 while M3 presented a southward flow. Thus the MC is narrow and centered above M2. The second situation (events 2 and 3) corresponded to a weak or southward flow at M2, a southward flow at M3 and a stronger alongshore flow at M1. Satellite images suggest that during these two events an eddy from the BC overshoot entered the array from east to west, pinching the MC (not shown).

3.2. Current Meter Statistics and Comparison With the WOCE Data Set

[19] Figure 5 shows means and variance ellipses for this data set and the previous one (1993–1995). The new data set provided information from above the 1000-m isobath near the supposed velocity maximum of the MC, information that was lacking because of the loss of a mooring in 1995 (VP99a). There, mean velocities were close to 40 cm s^{-1} at 500 dbars, whereas mean velocities for the upper current meter were slightly lower (36.2 cm s^{-1}). The strong mean velocities were oriented along isobaths and the major axes of the variance ellipses were along the isobaths. Moorings M2 and M3 were located near former moorings (OM5 for M2, OM6 and OM7 for M3) (Figure 1). M3, which was located between OM6 and OM7, showed means and variances that are compatible with those for former moorings. OM6 was still in the MC, with means exceeding standard deviations. It was still the case for the deeper level at M3 (C3,2 mean 12.5 cm s^{-1} and standard deviation 7 cm s^{-1}). The current meter at a depth of 150 dbars (C3,1) recorded only during 179 days and provided a mean slightly smaller than the variance. C3,2 also showed high variability during the first months. The main difference between the two data sets appeared in the standard deviations in the center of the array: they were smaller in 2001–2003 (6 cm s^{-1} at 217 m at M2) than in 1993–1995 (14.4 cm s^{-1} at 261 m at OM5). A part of the variance at OM5 was due to a lateral intrusion of warm subtropical water that lasted over a month in

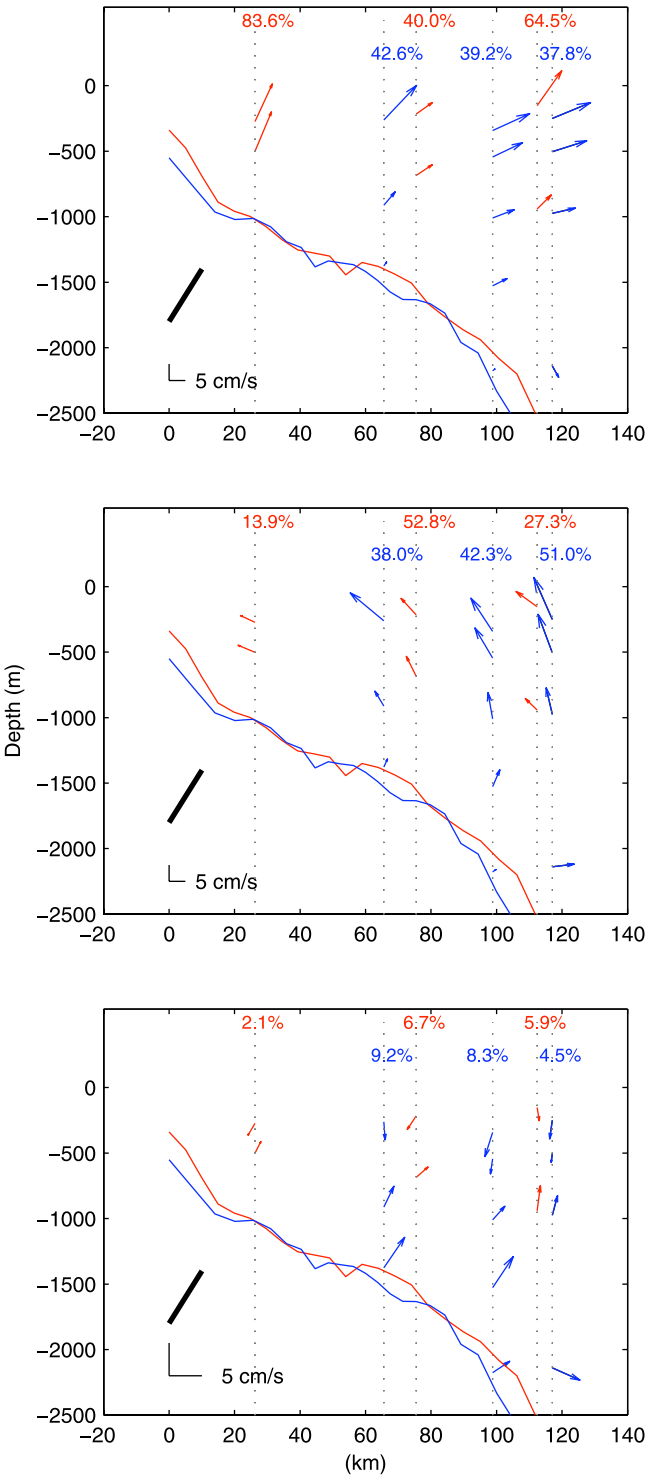

Figure 6. Empirical orthogonal functions (EOFs) with the percentage of total variance explained; in blue, from the WOCE time series (1993–1995), in red, from the CLIVAR time series (2001–2003). (top) Mode oriented along the mean flow ($EOF_{\parallel}$); (middle) mode transverse to the mean flow ($EOF_{\perp}$); (bottom) third mode (EOF3). Direction of isobaths is indicated by the thick solid line at bottom left.

August–September 1995 (VP99a). No such extreme event was recorded at M2. At mooring M1 the mean velocity at 500 m was slightly larger than the mean velocity at 270 m (39.5 versus 36.2 cm s^{-1} for the along-isobath component, 4.5 versus 4 cm s^{-1} for the cross-isobath component).

[20] A principal component analysis (PCA) provided an overview of the velocity field variations. It was performed on nonnormalized velocity anomalies, considering each mooring separately. The three leading empirical orthogonal functions (EOF) were coherent throughout the section and showed a mode of variation oriented along the mean flow ($EOF_{\parallel}$), a mode transverse to the mean flow ($EOF_{\perp}$), and a baroclinic mode directed along isobaths (EOF3) (Figure 6). These modes are similar to the ones observed in the previous data set (VP99a). Percentages of explained variance should be considered with caution, however. First of all, the time series data from M3 lasted only 179 days. Second, at M2, the time series was far from stationary with the strong cross-isobath event in December 2002 (if one considers only the first 12 months instead of the full 15 months, the percentage of variance explained by $EOF_{\perp}$ decreases from 53 to 30%). Furthermore, as there are only two current meters on each mooring, percentages cannot be compared directly with those from the 1993–1995 data set, for which the moorings carried more instruments.

[21] The predominant modes of variation above the 1000-m isobath were obtained for the first time and the along-isobath mode ($EOF_{\parallel}$) accounted for 83.6% of the total variance (Figure 6). The principal component associated with $EOF_{\parallel}$ at M1 had three peaks of energy above the 99% confidence level (CL), one centered at 180 days, another at 50–70 days, and a third at about 8 days (Figure 7). At M2, $EOF_{\parallel}$ showed a broad band of significant energy (above 99% CL) between 90 days and 200 days, with a peak at 180 days and sharp peaks (above 99% CL) at 9 and 6 days. Thus, in contrast to the findings of VP99a, a highly significant semi-annual peak was found for the along-isobath mode ($EOF_{\parallel}$) at M1 and M2. As the seasonality of the migration of the Brazil-Malvinas front is a recurrent question in the literature devoted to this region [e.g., *Saraceno et al.*, 2004], harmonic functions with annual and semiannual periods were tentatively fitted to the principal components, in spite of the shortness of the time series (Figure 7). At M1 the annual harmonic accounts for 29% of the variance of $EOF_{\parallel}$ and the semiannual harmonics, 16%. At M2, the percentages drop to less than 10% and the fit is not robust. The annual harmonic for $EOF_{\parallel}$ at M1 shows a maximum in May–June (end of austral autumn), thus suggesting a seasonal variation in the intensity of the MC above the 1000-m isobath.

[22] The cross-isobath variability ($EOF_{\perp}$) at M1 (only 13% of the total variance) exhibits a high-frequency energy content (marginal energy beyond 15 days) with significant peaks at 5 and 3.5 days, most likely caused by topographic waves (Figure 8). At M2 the cross-isobath variability (53% of the total variance) also had some energy at those short periods, but most of it was found in the 35–55 day band and around the semiannual period (Figure 8). VP99a fitted annual harmonics to the $EOF_{\perp}$ time series at OM5, OM6, and OM7: they were approximately in phase with maximum inshore flow in May–June and the fraction of explained variance accounted for by the harmonics increased consistently toward the deepest side of the current meter section. Here, annual and semiannual harmonics were fitted to $EOF_{\perp}$ at M2 (the time series at M3 was too short for this

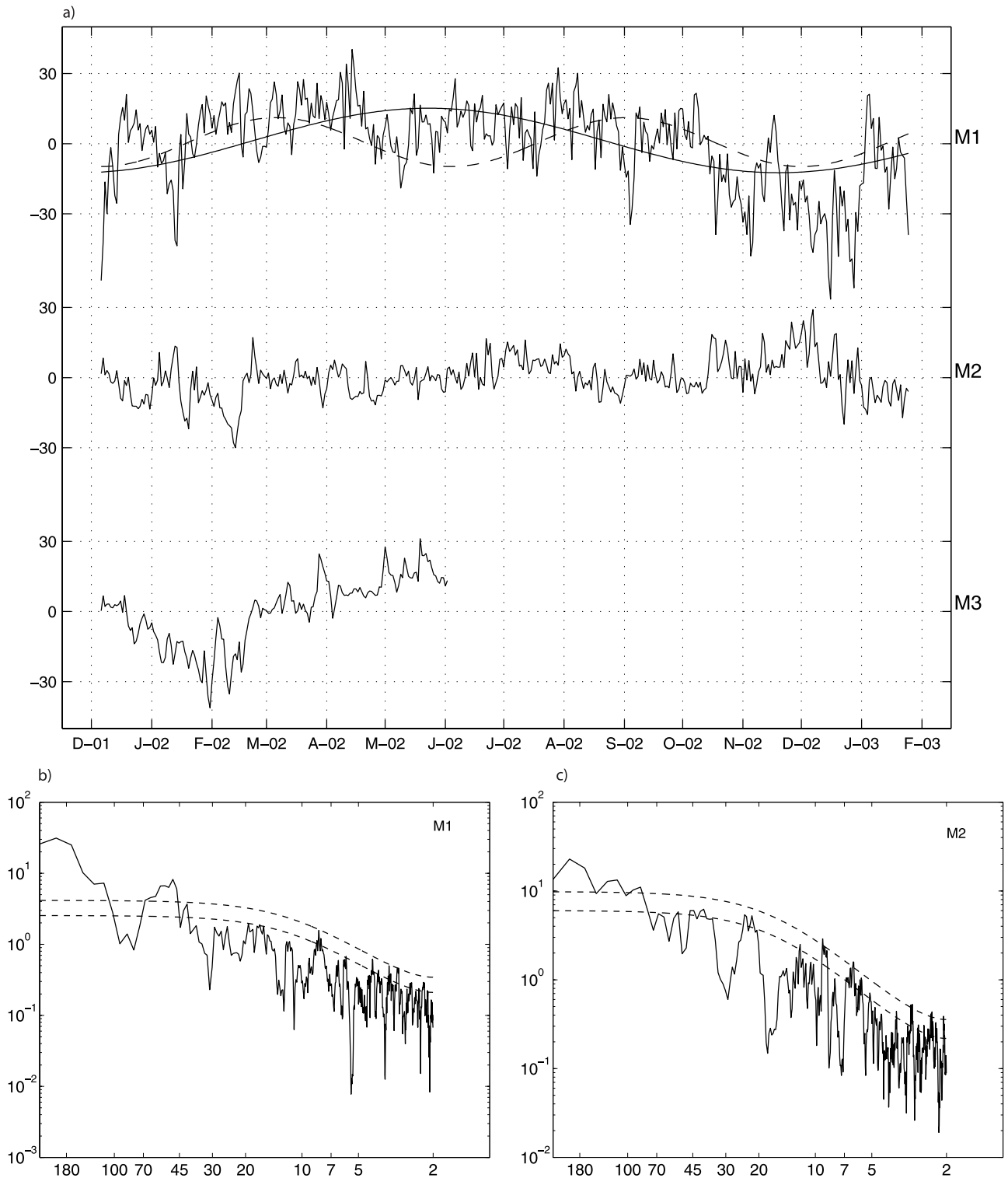

Figure 7. (a) Principal components associated with $EOF_{\parallel}$ at moorings M1, M2, and M3. Units are cm s^{-1}. Superimposed are the best fits for an annual and a semiannual harmonic at M1. (b) Power spectral densities of the principal component associated with $EOF_{\parallel}$ at M1; *x* axis is period in days. Dashed lines in spectra indicate 90% and 99% confidence levels. (c) As for Figure 7b at M2.

purpose) and explained 24% and 12% of the variance, respectively. As in VP99a, the maximum inshore flow was found in June at the end of austral autumn.

[23] The third mode accounted for a smaller fraction of the variance (2.1%, 6.7%, and 5.9% at M1, M2, and M3, respectively) (Figure 6). It was baroclinic and directed along isobaths. At M2 the spectrum of EOF3 showed two statistically significant (CL 99%) peaks at 8 and 4 days, suggesting waves trapped by the conjugated effects of bottom topography and stratification. Indeed, the third

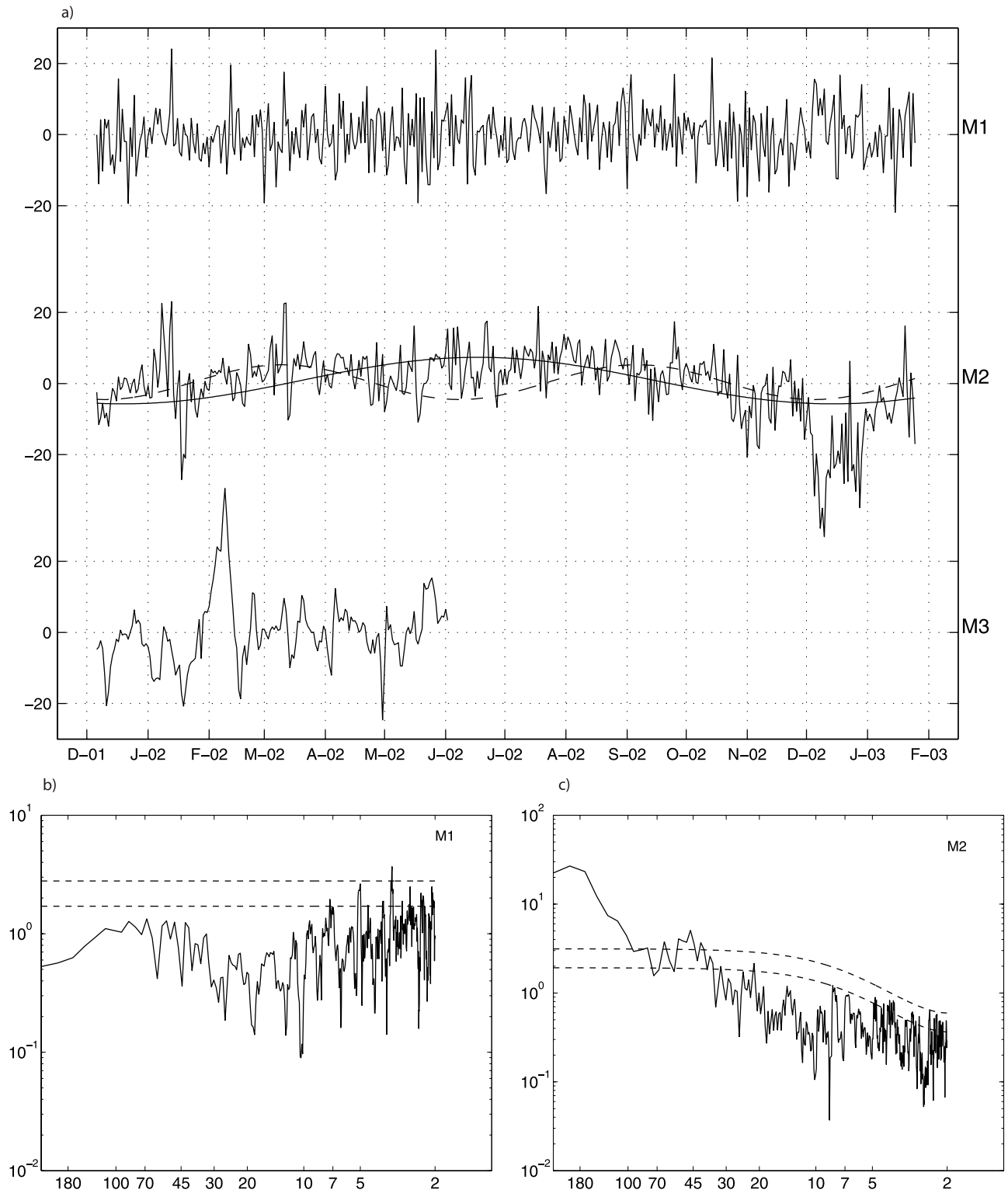

Figure 8. (a) Principal components associated with $EOF_{\perp}$ at moorings M1, M2, and M3. Units are cm s^{-1}. Superimposed are the best fits for an annual and a semiannual harmonic at M2. (b) Power spectral densities of the principal component associated with $EOF_{\perp}$ at M1; x axis is period in days. Dashed lines in spectra indicate 90% and 99% confidence levels. (c) As for Figure 8b at M2.

mode in the high-vertical-resolution array described by VP99a had a similar structure in the upper part of the water column and accounted for similar fractions of variance. It was bottom intensified and interpreted as the signature of waves trapped by the conjugated effects of topography and stratification.

[24] In summary, the new data set provided new information above the 1000-m isobath (M1 location) where a mooring was lost in 1993–1995 and suggested that means at M2 and M3 have not changed substantially since then. No signal of drift in the mean values was observed at M2 or M3. Therefore, we could compute a mean using the pooled current meter data. The spatial structure of variability had not changed either and similar modes of variation were observed. As expected, M3 was located near the eastern limit of the MC. As in 1993–1995, annual variations were observed in the cross-isobath component of the flow above the 1500-m isobath (M2) and none in the along-isobath component. The new data set showed that, above the 1000-m isobath, most of the velocity variation was along isobath (80% of the variance) and exhibited an annual cycle roughly in phase with the annual cycle of the cross-isobath component at M2 (maximum northward flow and maximum inshore flow around June).

4. Volume Transport Computation and Analysis

[25] The mean field $V_m(x, z)$ (equation (1) in section 2.2) is crucial for a proper computation of the transport variations. Current meters only provide subsurface measurements, yet it is essential to have a correct estimate of the mean surface velocity, as $V'(x, 0, t)$ (equation (1)) is the anomaly relative to this mean.

4.1. Volume Transport Estimates From Current Meters

[26] Daily maps of cross-section velocity were produced for the upper 1500 m using objective analysis with a Gaussian correlation function with a horizontal scale of 41 km and a vertical scale of 1135 m. Those scales were estimated from the 1993–1995 current meter array (appendix in VP99b). The grid of the map had a 2-km resolution in the horizontal and 25-m in the vertical planes. The error patterns associated with the objectively mapped velocity fields were sensitive to the spatial sampling of the data: largest errors were obtained on the edges and when distance between current meters exceeded the decorrelation scale (cf. VP99b, Figure 3). For transport estimates, only positive (equatorward) velocities are considered, rather than the algebraic sum of velocities across the section. The resulting error on the daily volume transport estimates from current meters in the upper 1500 m was 6 Sv for the first 254 days of the 1993–1995 deployment (4 Sv being attributable to the lack of data above the 1500-m isobath). The mean volume transport was 32.8 Sv for the first 254 days and 30.8 Sv if extended over 386 days.

[27] For the 2001–2003 deployment, the error in the daily volume transport was 4 Sv for the period during which C31 recorded (179 days), increasing to 7 Sv afterward. The error was approximately distributed as follows: 0.2 Sv inshore of M1, 1.2 Sv between M1 and M2 (distance 49 km), 1.2 Sv between M2 and M3 (distance 37 km), and 1.5 Sv to the east of M3. The mean transport was 32.0 Sv during the first 179 days 33.3 Sv if extended over 416 days.

[28] These rather short time series of daily transport derived from the current meters are used to validate the long altimetrically derived volume-transport time series (section 4.3).

4.2. Surface Velocity Estimates

4.2.1. Mean Surface Velocity Estimates

[29] In VP99b, mean surface velocity estimates $\langle V_{surface} \rangle$ were estimated in three ways: first, from a bicubic polynomial fit to the mean value derived from the current meter data; second, from the time average of the objective maps of cross-section velocity; and third, for intercomparison, computed as:

$$\langle V_{surface} \rangle = \langle V_{deep} \rangle + \langle V_{shear} \rangle$$

where $\langle V_{deep} \rangle$ is the mean velocity at the upper current meter and $\langle V_{shear} \rangle$ is the mean shear between the current meter depth and the surface. The time-averaged shear, $\langle V_{shear} \rangle$, was estimated from:

$$V_{surface} - \langle V_{surface} \rangle = V_{deep} - \langle V_{deep} \rangle + V_{shear} - \langle V_{shear} \rangle$$

where V_{shear} is the geostrophic shear estimate between the current meter depth and the surface provided by the hydrographic section from the Confluence 4 cruise (December–January 1994), $V_{surface} - \langle V_{surface} \rangle$ was the velocity anomaly from the T/P pass corresponding to the Confluence 4 hydrographic section (cycles 44 or 45), and $V_{deep} - \langle V_{deep} \rangle$ was the velocity anomaly obtained by subtracting the mean from the velocity recorded by the current meter at the time of the satellite pass. The nonsynchronicity of the hydrographic section and the satellite passes was certainly problematic, as were the different temporal and spatial scales relevant to each type of data, with their associated errors. However, a sensible mean surface velocity field could be derived (Figure 9).

[30] Unfortunately, we could not repeat the operation, since there were no hydrographic data available for the period of the 2001–2003 current meter mooring array. Instead, we used newly available surface drifter data. Sixty-four drifters went through the current meter array over the period 1994–2006. The corresponding data were used, as indicated in section 2.3, to estimate mean surface velocities (Table 2). The VP99b surface velocity estimates fell within the standard deviation of the drifter-derived velocities (Figure 9). Our new mean surface velocity estimates hardly differed from those of VP99b.

4.2.2. Variation in the Surface Currents and Width of the MC

[31] A time series of the cross-track surface geostrophic velocity was then computed from the mean surface velocity derived above and the SGVA derived from altimetry (Figure 10a). It provided further insight into the surface velocity variation since October 1992 and particularly during the two mooring deployment periods. It shows a quite stable flow in spite of a few outstanding aperiodic events during which equatorward surface velocities were weak. The MC however was never totally cut off. One such event, which occurred at the end of August 1994 and lasted about a month, and is described by VP99a, was a meander from the BC that entered the current meter array from east to west, pinching the MC with no inshore acceleration. Another outstanding event was seen around 20 September 2001: there were hardly any positive surface velocities, and

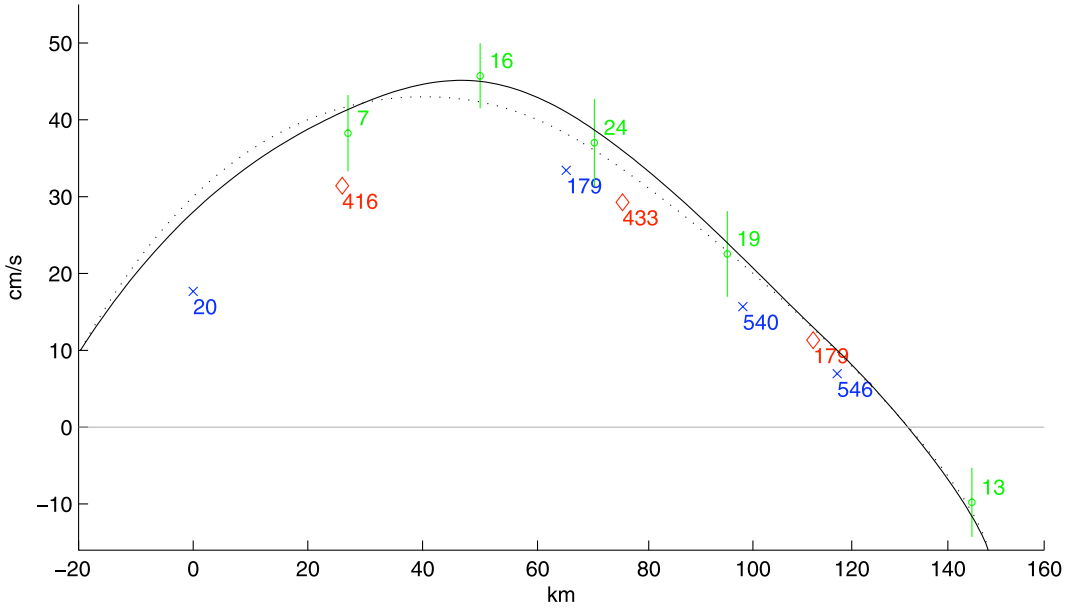

Figure 9. Mean cross-track surface velocity. Dotted black line: mean surface velocity chosen for the transport computation in VP99b; full black line: mean surface velocity chosen here. In green: surface velocities from drifters. Mean velocity for the shallowest instrument at each mooring: blue cross for 1993–1995; red diamond for 2001–2003. Number of data days is indicated.

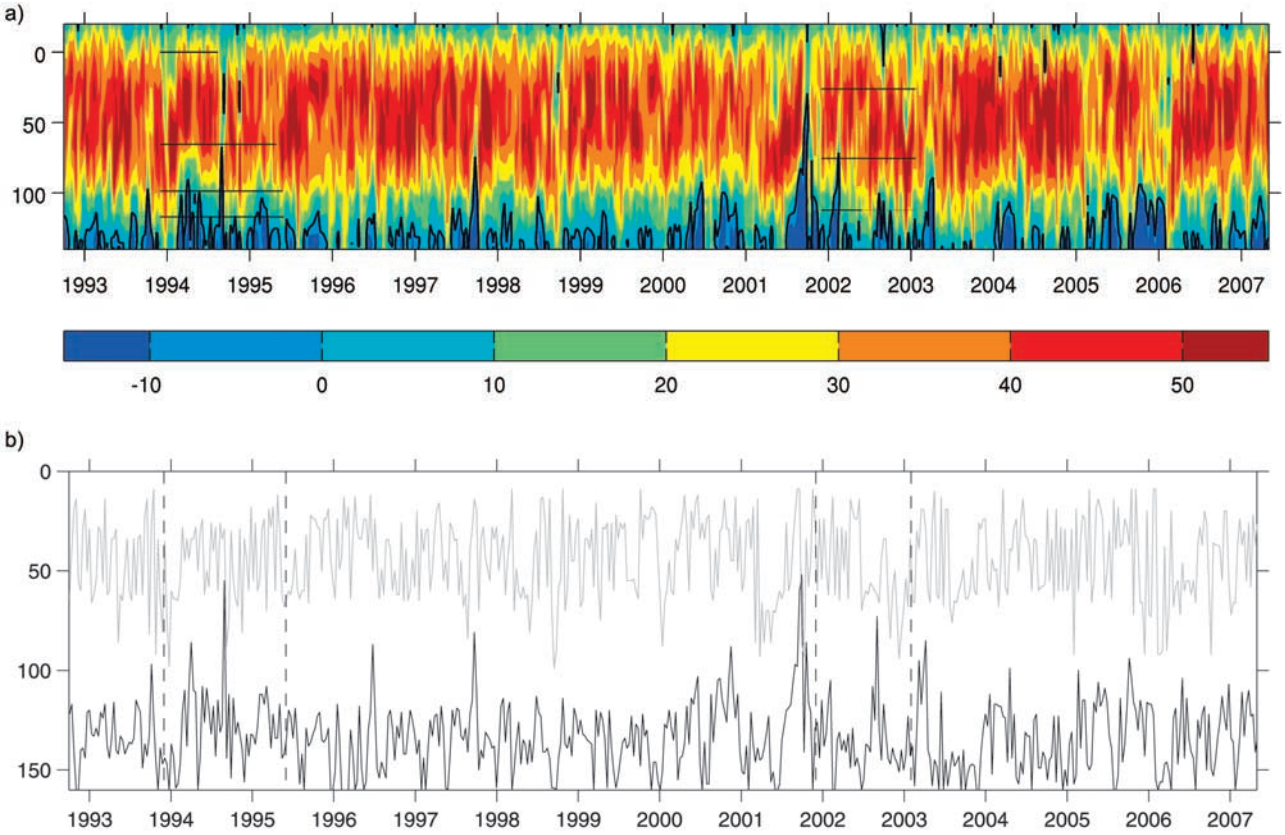

Figure 10. (a) Surface velocity across the section as a function of time; *x* axis is time in calendar years; *y* axis is distance along track in kilometers, the origin being the M1 location. Units for color bar: cm s^{-1}. The time-space location of the in situ observations is indicated by black lines. (b) Location of the maximum surface velocity as a function of time (gray) and the width of the MC as a function of time. The ordinal units are in kilometers. For the location of the maximum surface velocity, the distance is from the M1 mooring site and along Jason track 26.

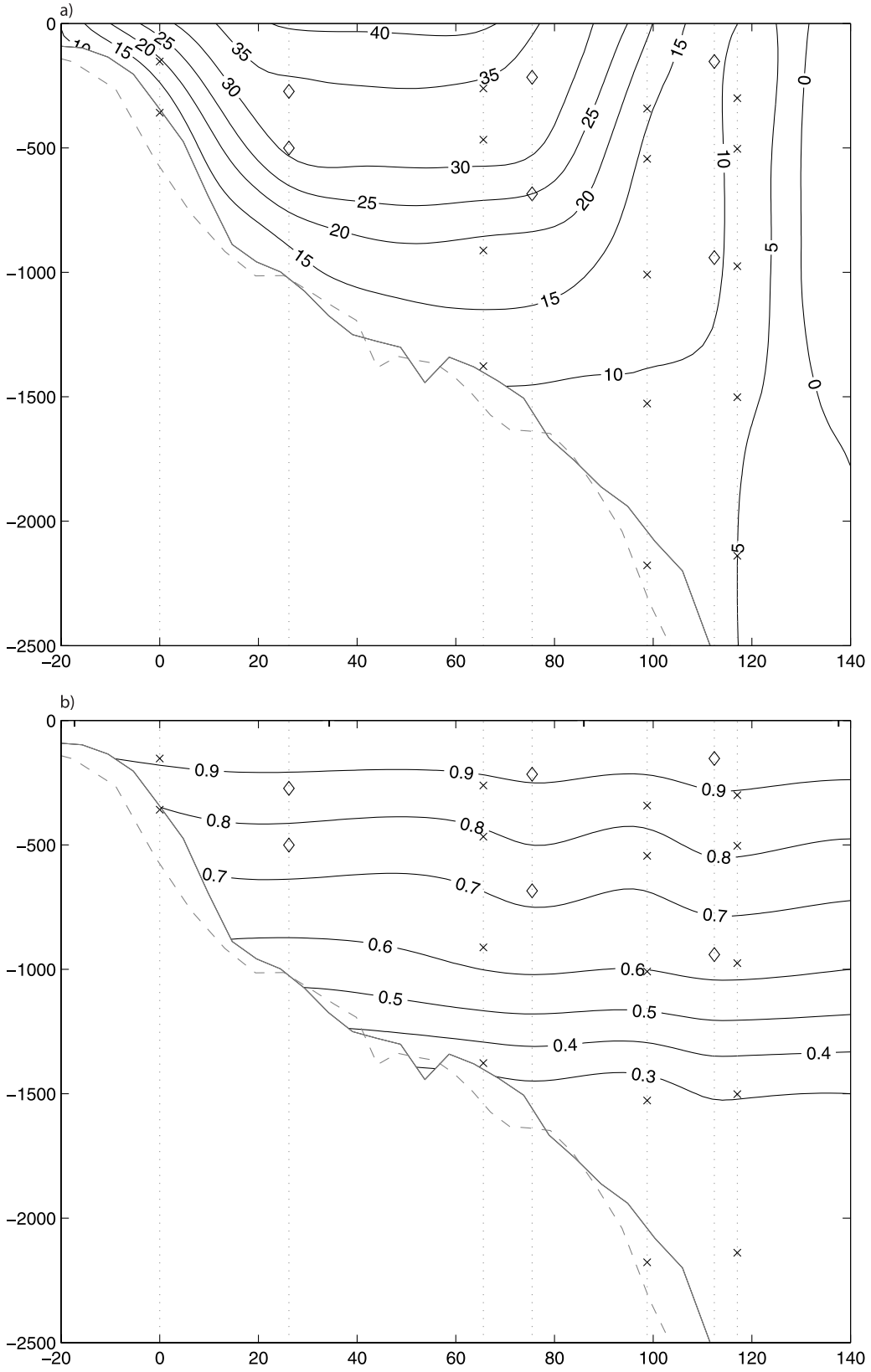

Figure 11. (a) Mean velocity field across the section in cm s^{-1}. The ordinal scale is the depth in meters; the abscissal scale is the distance in kilometers. Crosses correspond to location of current meters in 1993–1995; diamonds correspond to location of current meters in 2001–2003. (b) Correlation between the data from the uppermost current meters and those from the underlying instruments. The correlation coefficient is normalized to unity at the surface.

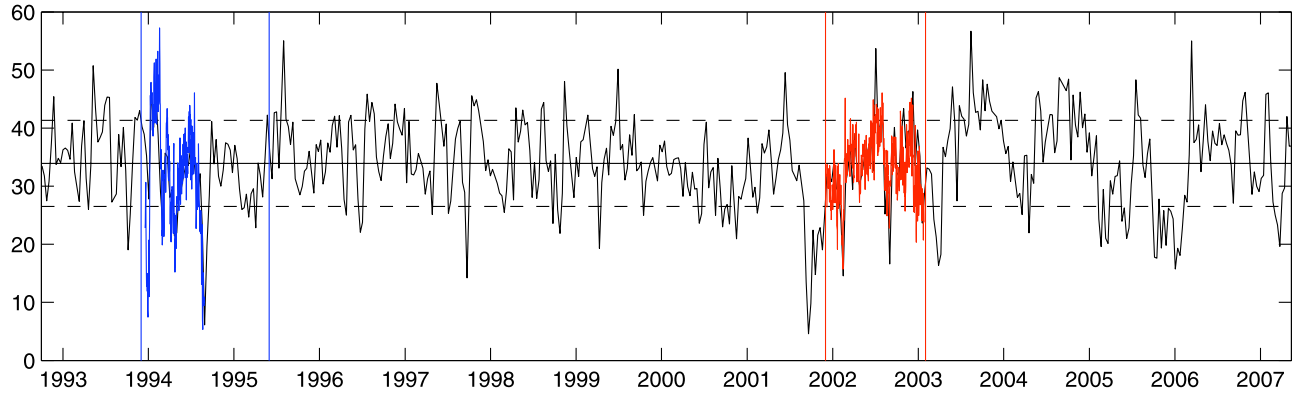

Figure 12. Transport (in Sv) in the upper 1500 m computed from altimetric data (in black) versus transport computed from in situ measurements (in blue for 1993–1995 and in red for 2001–2003).

again a meander from the BC entered the mooring array from east to west.

[32] Surface velocity maxima exceeded 50 cm s^{-1}. The core of the MC surface flow fluctuated over a distance of 80 km between the 1000- and 1800-m isobaths (Figure 10b). Its average location was 45 km (above the 1200-m isobath). The estimated width of the MC was based on the MC surface water flowing equatorward with a velocity greater than 5 cm s^{-1} (Figure 10b). The mean value was 134 km and, 9% of the time, the width exceeded the lateral extension (160 km) over which we computed the transport. A careful examination of the transport values (see following paragraph) showed that while transport and width were highly correlated (correlation coefficient greater than 0.7) for width values smaller than 140 km, the correlation dropped to 0 for widths larger than 140 km. We noted that width, maximum velocity, and location of the maximum velocity were not significantly correlated (correlation coefficients less than 0.2).

4.3. Calculation and Validation of the MC Transport Time Series

[33] Across the section we considered positive (equatorward; that is MC) and negative transport (return flow) as separate quantities; therefore the mean velocity will influence transport estimates more than a simple offset would do.

[34] As the means from two in situ time series were coherent, we constructed a mean velocity field $V_m(x, z)$ from both current meter data sets (Figure 11a) using a bicubic polynomial fit to the mean values of velocities perpendicular to the section. The 2001–2003 data set provided new information on the vertical structure of the current in the center of the array, in which a 60-km gap between OM1 and OM5 had to be extrapolated by VP99b. Mean velocities observed by M1 were slightly larger (4 cm s^{-1}) at depth and slightly smaller (−1 cm s^{-1}) at the first subsurface level than those extrapolated by VP99b. At M2 differences from OM5 were negligible (below 1 cm s^{-1}, but larger near the surface and smaller below). At M3, velocities near 1000 m depth were larger by about 5 cm s^{-1} in this region, which is invaded aperiodically by meanders or eddies from the Brazil Current.

[35] The estimated mean transport in the upper 1500 m using the two data sets was 32.6 Sv; i.e., 1.1 Sv higher than the one obtained using the 1993–1995 data set (with the bicubic spline interpolation). The mean net volume transport derived from the current meters in the upper 1500 m was 32.8 Sv during the first 254 days of the 1993–1995 deployment, and extending the estimates over a longer period (386 days) led to a slightly lower transport by 2 Sv (section 4.1). During the 2001–2003 deployment period, the mean transport estimate was 32.0 Sv for the first 179 days and 33.3 Sv for 416 days. These different estimates of mean northward transport in the upper 1500 m are coherent.

[36] The function A(x, z) reflecting the vertical structure of the current was computed from the correlation coefficient between the uppermost instruments and instruments at depth. The correlation coefficient was normalized to unity at the surface and mapped over the section (Figure 11b). It is quite similar to the one extrapolated over the 60-km gap in VP99b.

[37] The MC volume transport in the upper 1500 m was then computed from the altimetric data from October 1992 to May 2007. It was compared to the transport derived from in situ measurements for the period 1993–1995 (the first 254 days) and for the period 2001–2003 (the first 179 days for which data from C3,1 are available) estimated from daily objective maps of velocity orthogonal to the section (Figure 12). The in situ transport estimates were low-pass-filtered with a 20-day cutoff period and resampled at the satellite date. The correlation coefficient between the altimetrically derived transport and the in situ transport exceeded 0.7 in both periods, well above the 95% confidence level of 0.48. The root mean square difference between the current meter-derived volume transport and the altimetrically derived transport was 5.6 Sv for the first 254 days of the 1993–1995 deployment (to be compared to the 6 Sv error estimate on the current meter-derived transport; see section 4.1), 4.7 Sv for the first 179 days of the 2001–2003 deployment (error estimate of 4 Sv in the current meter-derived transport) and 5.2 Sv for the whole 2001–2003 period (error estimate of 7 Sv in the current meter-derived transport). Thus the good agreement between the transport derived from altimetry and the transport derived from the in situ data obtained in 1993–1995 was also found with the 2001–2003 data set 8 years later. We then analyzed the variations of the MC transport from the intraseasonal to the interannual timescale.

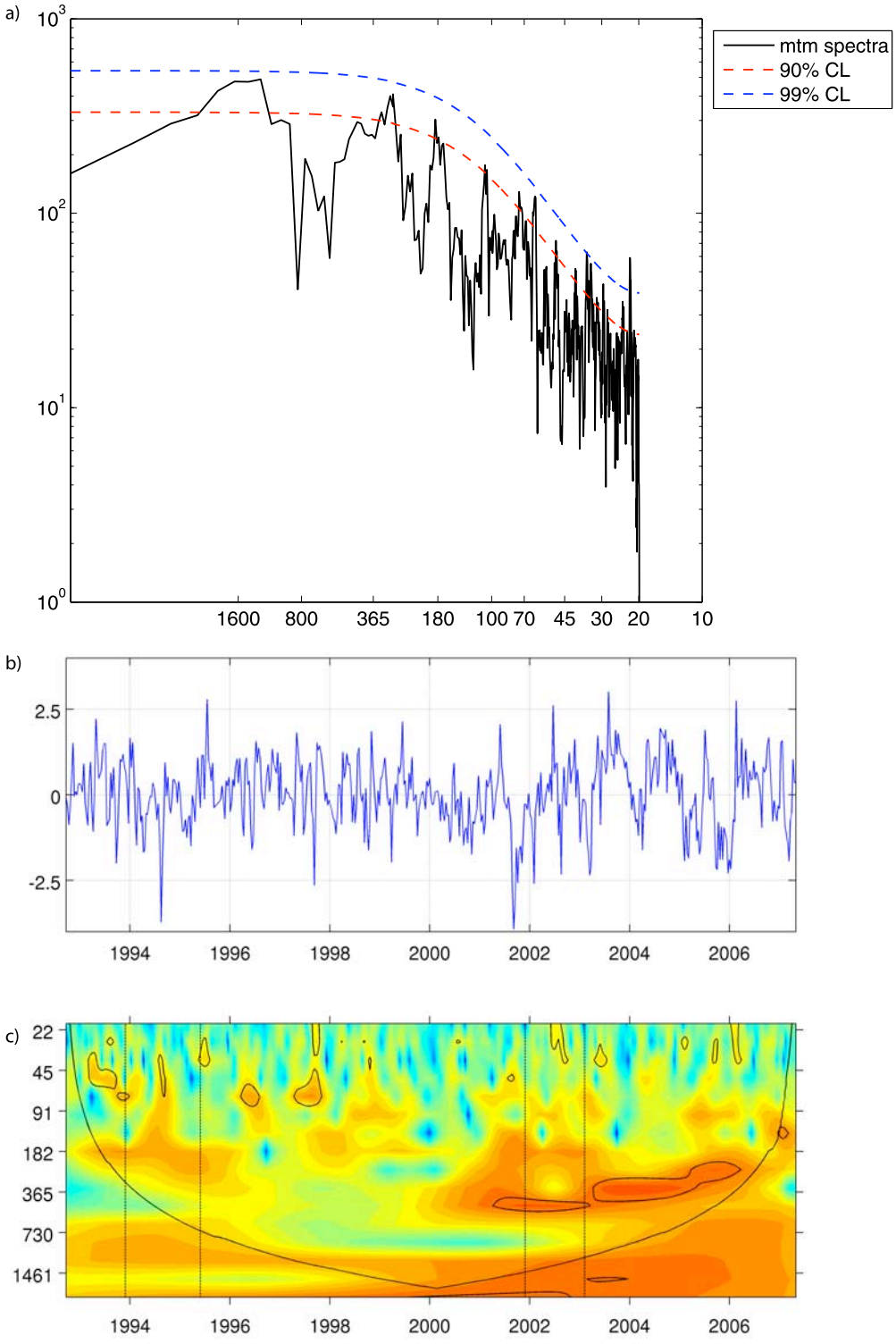

Figure 13. (a) Spectrum of the altimetrically derived volume transport time series. Confidence limit intervals 90% and 99%; *x* axis is period in days. (b) Normalized altimetrically derived volume transport time series, and (c) the corresponding wavelet transform amplitude; *y* axis is period in days. The black lines indicate the 95% CL and the cutoff region to avoid edge effects.

4.4. Variation in the MC Volume Transport

[38] The mean volume transport was 34.3 Sv, with a standard deviation of 7.4 Sv. The mean over the 14 years was slightly larger than the mean derived from the current meter data. Indeed, both current meter deployment periods corresponded to a slightly weaker than average flow.

[39] A few strong and apparently aperiodic peaks, due to the considerable mesoscale activity close to the confluence,

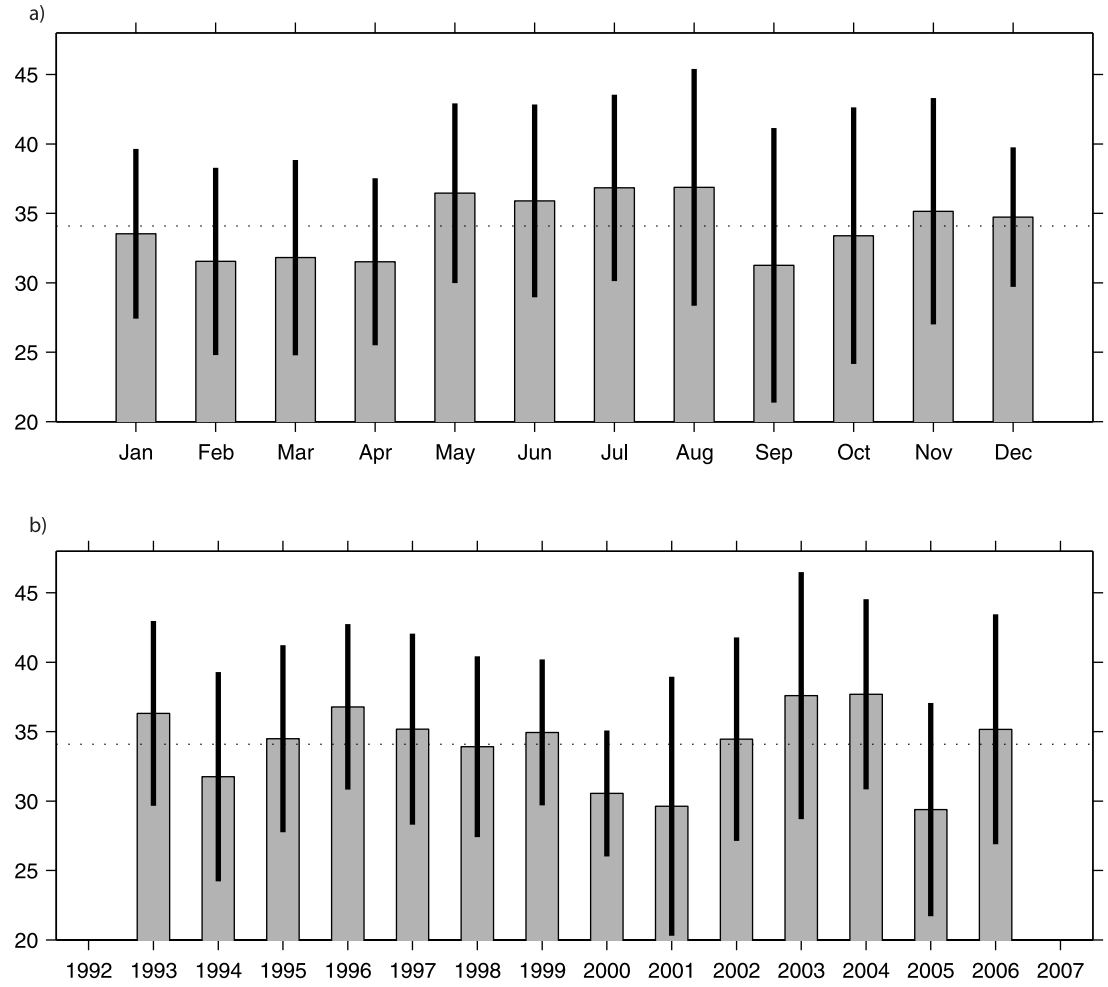

Figure 14. (a) Monthly and (b) yearly averages of the MC altimetrically derived transport in the upper 1500 m from January 1993 to December 2006; y axis units are Sverdrup (10^6 m^3 s^{-1}). The standard deviation is shown by the black line centered on each bar. Mean transport for 1993–2006 is indicated by the dotted line.

were found in the volume transport time series (Figure 12). The drastic decreases in transport below 10 Sv, as in September 1994 and in September–October 2001, were concomittant with east-to-west incursions of meanders or eddies from the Brazil Current, as already described in section 4.2.2 on the surface velocity.

[40] A few maximum peak values in the transport exceeded 55 Sv and although the time series of volume transport and of the width of the MC at the surface were correlated (correlation coefficient of 0.63), these extreme peaks did not correspond to a large MC width but rather to peaks in the surface velocity. The volume transport time series was extremely well correlated (correlation coefficient larger than 0.9) with the time series of mean surface geostrophic velocity anomaly between isobaths 1000 m and 1500 m, which may not be so surprising, considering equation (1) (section 2.2).

[41] The surge of isolated events accounted for a part of the variability. However, the transport time series exhibited interesting spectral features. In situ and satellite-derived transport estimates covered different spectral ranges. The spectrum of the transport time series derived from the 1993–1995 current meter array showed peaks at a relatively high frequency (8 days) associated with bottom-trapped topographic waves (VP99a), at about 30 days, at periods from 50 to 80 days, and close to the semiannual period (VP99b). The transport time series derived from the 2001–2003 set of current meter data had a similar distribution of energy, with salient peaks at high frequency (6 and 8 days), at about 25 days, at about 40 days, at a period from 60 to 120 days, and in a broad band centered at about 180 days (not shown). The 14-year-long altimetrically derived transport time series exhibited a spectral content similar to that of the short current meter-derived transport time series for intraseasonal variations, with salient peaks at about 23 days and 35 days, with most of the energy concentrated at periods from 55 to 120 days and close to the semiannual period. It also showed some energy in a band at around 300 days, including the annual period (Figure 13a). In contrast to the findings of VP99b and VPM, there is some energy at the annual period.

[42] A wavelet analysis of the altimetrically derived transport time series showed the time modulation of the spectral content (Figure 13b). The content of energy at the

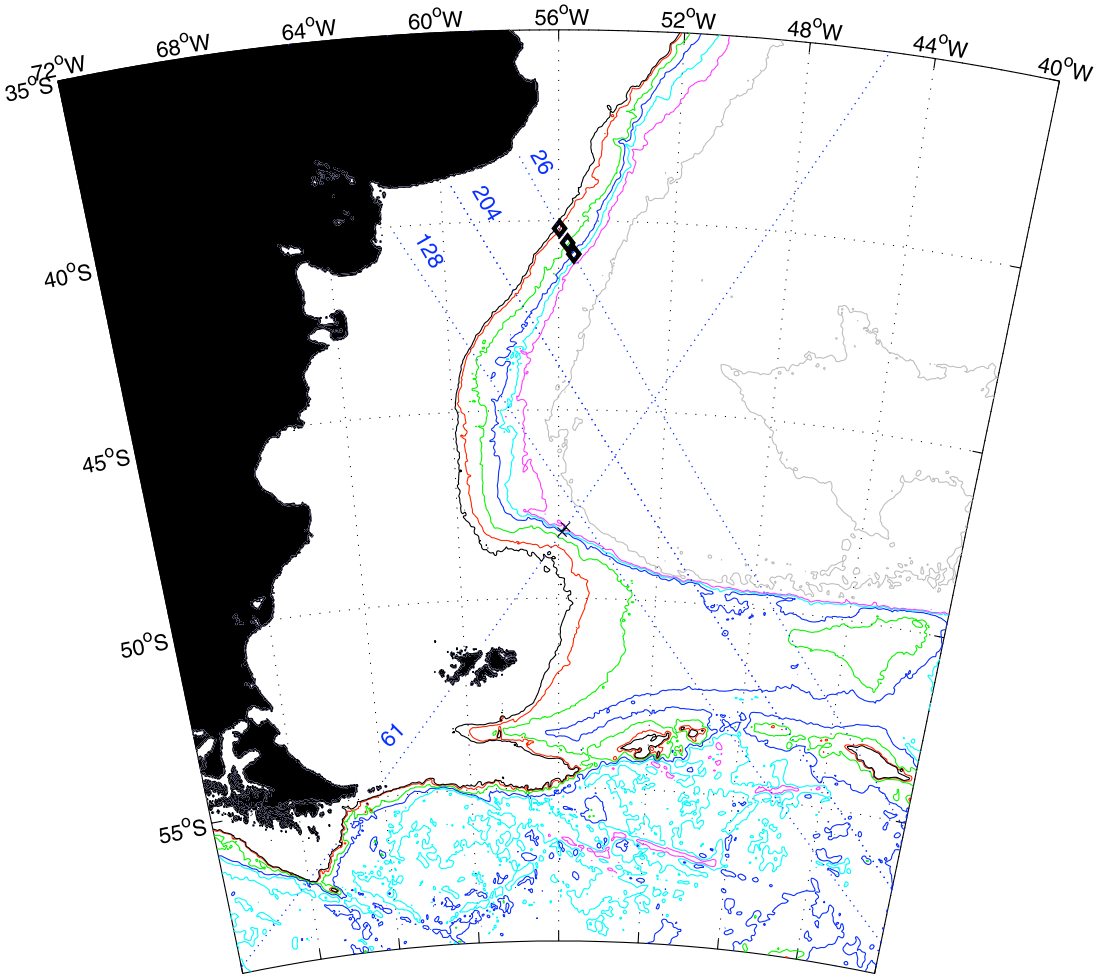

Figure 15. Selected f/H contours: black: -1.4×10^{-7} m s^{-1}, red: -10^{-7} m s^{-1}, green: -0.6×10^{-7} m s^{-1}, dark blue: -0.4×10^{-7} m s^{-1}, light blue: -0.3×10^{-7} m s^{-1}, pink: -0.25×10^{-7} m s^{-1}, gray: -0.192×10^{-7} m s^{-1}. The Malvinas Current flows between f/H contours -1.5×10^{-7} and -0.4×10^{-7}. T/P and Jason-1 ground tracks 26, 204, 128, and 61 are suitably oriented, departing less than 30° from the perpendicular to the f/H contours.

annual and semiannual periods varied with time. During the 1993–1995 deployment there was some energy near the semiannual period but very little at the annual period, in agreement with VP99b. In contrast, during the 2001–2003 deployment, energy at the annual period was important. From 1992 to the end of 2000 there was little energy around the annual period, whereas from 2001 on, energy was concentrated in a wide spectral band, including the semiannual and annual periods. Thus, a change in the spectral composition of transport variations occurred in 1999–2000, with a concentration of energy around the annual period.

[43] In spite of the nonstationary nature of the time series, we computed monthly transport averages (Figure 14a). The semiannual modulation was clear, with two minima during the year: one in April and a second one in September (31 Sv). The annual modulation was also visible although noticeably weaker, with strongest flows (37 Sv) during austral winter months (July and August).

[44] Interannual variability was also important and yearly averages of volume transport ranged from a minimum of 29 Sv in 2005 to a maximum of 38 Sv in 2004 (Figure 14b). The temporal evolution of these yearly averages of volume transport could suggest a low-frequency modulation with an 8-year timescale, except for the minimum in 2005.

5. Summary and Discussion

[45] The new current meter data (2001–2003) gathered 8 years after the first set (1993–1995) did not reveal any trend in the mean and the other related statistical parameters but rather provided new information on the water column above the 1000-m isobath, in which a mooring had been previously lost. Most of the flow variations above 1000 m were orientated along the isobath direction and presented a significant annual component (30% of the variance). This annual cycle was in phase with the seasonal pivoting of the Brazil-Malvinas front, with an along-shore migration of about 300 km along the 1000-m isobath, described by *Saraceno et al.* [2004, 2005].

[46] The observations above the 1000-m isobath validated the extrapolation made by VP99b to fill the gap due to the mooring loss. The 2001–2003 data set confirmed

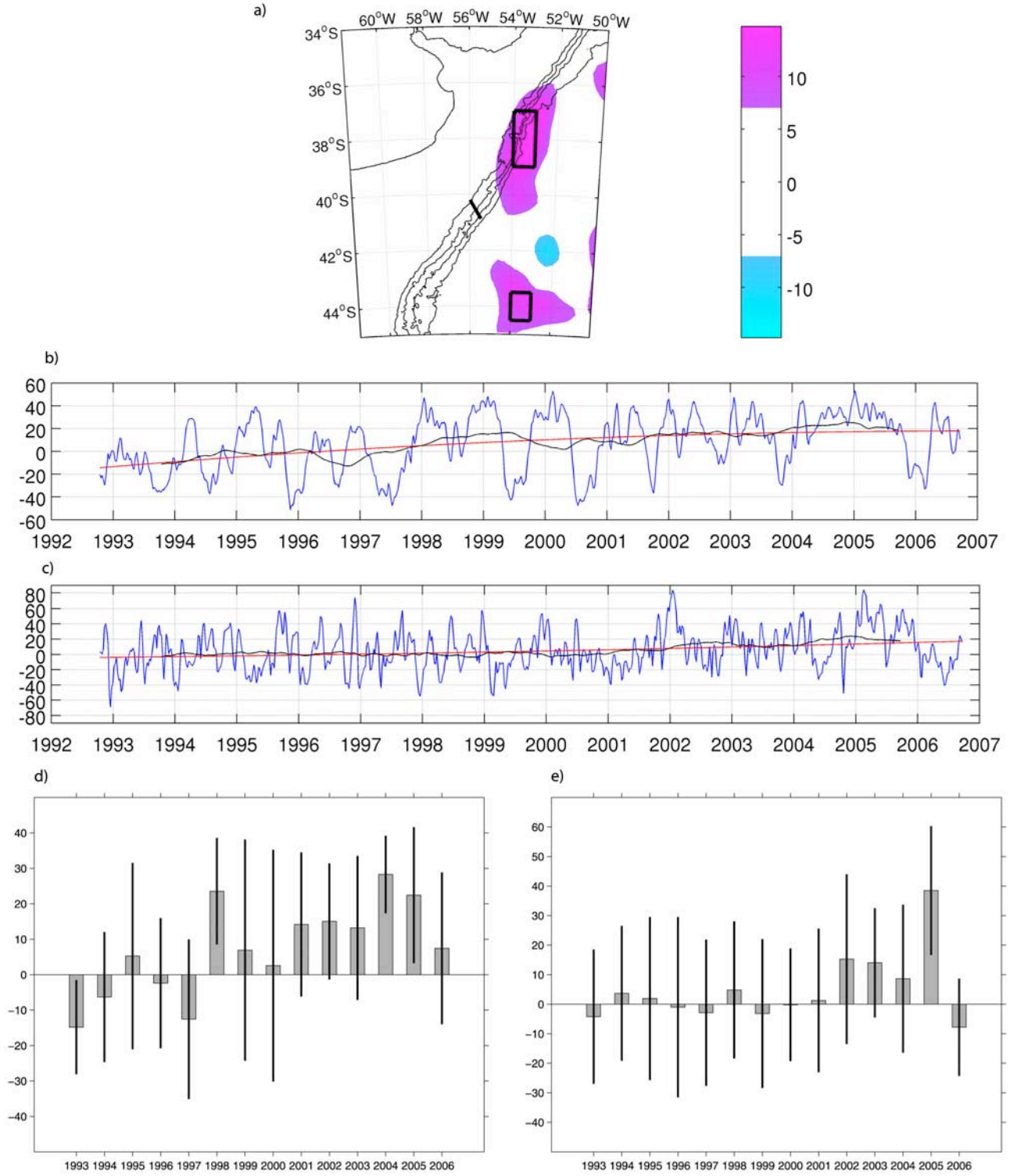

Figure 16. Sea level anomalies near the Brazil-Malvinas Confluence. (a) Difference between the SLA averaged over the period from 1 January 2000 to December 2006 and the SLA averaged from January 1993 to December 1999. Units are in centimeters. (b) Time series of SLA averaged over a box delimited by 37°–39°S and 53°–54°W: in blue, full time series (at a resolution of 7 days); in black, a 2-year running mean, in red, a second-degree polynomial trend. (c) Same as for Figure 16b, but over a box delimited by 44.5°S and 43.5°S and 54°–53°W. (d and e) Annual means of SLA over the two boxes, with Figure 16d corresponding to Figure 16b and Figure 16e corresponding to Figure 16c. The standard deviation is shown by a black line centered on each bar.

that the deployment of a mooring at the M2 location (above the 1500-m isobath) is important as the velocity from the shallow current meter at this location is highly correlated with the MC transport. Mean values and flow structure were similar for the two deployments periods. A 14-year-long time series of the Malvinas Current volume transport was produced. Over the 14 years, its spectral content exhibited an evolution with, in particular, the appearance of energy in a spectral band that included the annual period.

[47] A few questions arise. Is the observed variation in transport at 41°S representative of MC variation or is it an artifact due to the formidable mesoscale activity at the confluence? What is the origin of this variation? Is it local, because of the proximity of the Confluence? Is it remotely forced? Complete answers to these questions are beyond the scope of this paper. However, we will show that altimetry indicates that changes occurred in the whole of the SW Atlantic around 2000.

[48] We showed in section 4.4 that the mean SGVA between the 1000- and 1500-m isobaths along track 26 was highly correlated ($r > 0.9$) with the volume transport of the MC. The MC flows along f/H contours, and the two isobaths, 1000-m and 1500-m, correspond roughly to f/H contours -10×10^{-8} and -6.4×10^{-8} m s^{-1}, respectively. We computed time series of SGVA averaged between the same f/H contours on tracks 204, 128, and 61, which are upstream of track 26, and are suitably oriented, departing less than 30° from the perpendicular to the f/H contours (Figure 15). These time series can be considered as rough proxies for MC variations. All the time series of transport proxies showed a change in their spectral content with the appearance of a seasonal cycle around year 2000, thus indicating a change over the whole course of the MC (not shown). From October 1992 to October 1997, MC transport variations were predominantly semiannual and seemed to follow a time-varying Sverdrup balance responding in less than 20 days to changes in the wind stress curl north of 50°S mostly in the Pacific sector (VPM). Has the wind changed? Indeed, preliminary examination of the NCEP reanalysis wind product suggested that the annual cycle in the wind stress curl over the Pacific north of 50°S was larger than usual from 2001 to 2007. This may be the beginning of an answer.

[49] Were changes also observed in the Brazil Current close to the confluence around year 2000? Differences in mean sea level anomalies before year 2000 and after year 2000 show a significant increase (up to 10 cm) in mean SLA north of 40°S along the continental slope, which would be indicative of a southern shift of the confluence (Figure 16a). The temporal evolution of SLA at the location of the maximum difference (37°–39°S and 53°–54°W) exhibits seasonal variations, and both a 2-year running mean and a second-degree polynomial fit suggest a general trend with an increase of more than 20 cm from 1993 to 2006 (Figure 16b). However, annual means of SLA at the same location bear no clear relationship to the annual means of the MC volume transport (Figure 16d and Figure 14b). The SLA difference map (Figure 16a) features another maximum in the region of the Brazil Current overshoot. The time series of the SLA at the location of this secondary maximum (43°–45°S and 53°–54°W) contains high frequencies, and similarly a 2-year running mean or a second-degree polynomial fit suggests a trend with an increase (of about 15 cm in 13 years; Figure 16c). The SLA annual means (Figure 16e) point to a significantly stronger than usual Brazil Current overshoot from 2002 to 2005, with, in particular, an exceptionally high anomaly in 2005 (mean value 38 cm) simultaneous with the weakest annual mean MC transport (Figure 14b). Thus, the years during which the MC transport variations had energy concentrated around the annual period (2001 to 2006) correspond to years with an anomalously southern location for the Brazil-Malvinas Confluence and the Brazil Current overshoot.

[50] *Garzoli and Giulivi* [1994] suggested that interannual variability in the Confluence might be caused by anomalous patterns of wind stress curl in the southwest Atlantic south of the Confluence. Analyses of correlations and coherences between the MC transport and the wind stress curl over the southern hemisphere and between the MC transport and the sea level anomalies over the southern ocean are in progress in order to determine whether and to what extent the observed interannual variability has a local or a remote cause.

[51] **Acknowledgments.** The authors are indebted to Ray Griffiths for his valuable comments on the manuscript. They gratefully thank Nathalie Sennechael, Annie Kartavtseff, Juliette Mignot, and Nicolas Barré (LOCEAN, Paris) for their help. The Servicio de Hidrografía Naval (Buenos Aires, Argentina) permitted the deployment and recovery cruises aboard the R/V *Puerto Deseado*. The cooperation of the crew members of the R/V *Puerto Deseado* is warmly acknowledged. The altimeter products were produced by Ssalto/Duacs and distributed by Aviso, with support from the Centre National d'Etudes Spatiales. This work is part of the French contribution to CLIVAR. It was funded by CNES and by CNRS (Centre National de la Recherche Scientifique).

References

Agra, C., and D. Nof (1993), Collision and separation of boundary currents, *Deep Sea Res., Part I*, *40*, 2259–2282, doi:10.1016/0967-0637(93)90103-A.

Barré, N., C. Provost, and M. Saraceno (2006), Spatial and temporal scales of the Brazil-Malvinas Confluence documented by simultaneous MODIS Aqua 1.1-km resolution SST and color images, *Adv. Space Res.*, *37*(4), 770–786, doi:10.1016/j.asr.2005.09.026.

Brambilla, E., and L. D. Talley (2006), Surface drifter exchange between the North Atlantic subtropical and subpolar gyres, *J. Geophys. Res.*, *111*, C07026, doi:10.1029/2005JC003146.

Garzoli, S. (1993), Geostrophic velocity and transport variability in the Brazil-Malvinas Confluence, *Deep Sea Res., Part I*, *40*, 1379–1394, doi:10.1016/0967-0637(93)90118-M.

Garzoli, S., and Z. Garraffo (1989), Transports, frontal motions and eddies at the Brazil-Malvinas currents confluence, *Deep Sea Res., Part A*, *36*(5), 681–703, doi:10.1016/0198-0149(89)90145-3.

Garzoli, S., and C. Giulivi (1994), What forces the variability of the southwestern Atlantic boundary currents?, *Deep Sea Res., Part I*, *41*, 1527–1550, doi:10.1016/0967-0637(94)90059-0.

Goni, G. J., and I. Wainer (2001), Investigation of the Brazil Current front variability from altimeter data, *J. Geophys. Res.*, *106*, 31,117–31,128, doi:10.1029/2000JC000396.

Goni, G. J., S. Kamholz, S. Garzoli, and D. Olson (1996), Dynamics of the Brazil-Malvinas Confluence based on inverted echo sounders and altimetry, *J. Geophys. Res.*, *101*, 16,273–16,298, doi:10.1029/96JC01146.

Gordon, A. L., and C. Greengrove (1986), Geostrophic circulation of the Brazil-Malvinas Confluence, *Deep-Sea Res.*, *33*, 573–585, doi:10.1016/0198-0149(86)90054-3.

Kartavtseff, A. (2005), Current meter measurements 2001–2003, *Data Rep. 4/05*, Lab. d'Oceanogr. et du Climat: Exp. et Approches Numer., Paris.

Killworth, P. D. (1992), An equivalent-barotropic mode in the Fine Resolution Antarctic Model, *J. Phys. Oceanogr.*, *22*, 1379–1387, doi:10.1175/1520-0485(1992)022<1379:AEBMIT>2.0.CO;2.

Lebedev, L., and D. Nof (1997), Collision of boundary currents: Beyond a steady state, *Deep Sea Res., Part I*, *44*, 771–779, doi:10.1016/S0967-0637(96)00127-6.

Maamaatuaiahutapu, K., V. Garçon, C. Provost, and H. Mercier (1998), Transports of the Brazil and Malvinas Currents at their Confluence, *J. Mar. Res.*, *56*, 417–438, doi:10.1357/002224098321822366.

Matano, R. P. (1993), On the separation of the Brazil Current from the coast, *J. Phys. Oceanogr.*, *23*, 79–90, doi:10.1175/1520-0485(1993)023<0079:OTSOTB>2.0.CO;2.

Matano, R. P., M. G. Schlax, and D. B. Chelton (1993), Seasonal variability in the southwestern Atlantic, *J. Geophys. Res.*, *98*, 18,027–18,035, doi:10.1029/93JC01602.

Niiler, P. P., and J. D. Paduan (1995), Wind-driven motions in the northeast Pacific as measured by Lagrangian drifters, *J. Phys. Oceanogr.*, *25*, 2819–2830.

Olson, D. B., G. P. Podesta, R. H. Evans, and O. B. Brown (1988), Temporal variations in the separation of Brazil and Malvinas Current, *Deep Sea Res., Part A*, *35*(12), 1971–1990, doi:10.1016/0198-0149(88)90120-3.

Peterson, R. G. (1992), The boundary currents in the western Argentine basin, *Deep Sea Res.*, *39*, 623–644, doi:10.1016/0198-0149(92)90092-8.

Peterson, R. G., and L. Stramma (1991), Upper-level circulation in the South Atlantic Ocean, *Prog. Oceanogr.*, *26*(1), 1–73, doi:10.1016/0079-6611(91)90006-8.

Piola, A. R., and A. L. Gordon (1989), Intermediate water in the southwest South Atlantic, *Deep Sea Res.*, *36*, 1–16, doi:10.1016/0198-0149(89)90015-0.

Provost, C., and P.-Y. LeTraon (1993), Spatial and temporal scales in altimetric variability in the Brazil-Malvinas Confluence region: Dominance of the semiannual periods and large spatial scales, *J. Geophys. Res.*, *98*, 18,037–18,061, doi:10.1029/93JC00693.

Provost, C., O. Garcia, and V. Garçon (1992), Analysis of satellite sea surface temperature time series in the Brazil-Malvinas Confluence region: Dominance of the annual and semi-annual periods, *J. Geophys. Res.*, *97*, 17,841–17,858, doi:10.1029/92JC01693.

Saraceno, M., C. Provost, A. R. Piola, J. Bava, and A. Gagliardini (2004), The Brazil Malvinas Frontal System as seen from nine years of AVHRR data, *J. Geophys. Res.*, *109*, C05027, doi:10.1029/2003JC002127.

Saraceno, M., C. Provost, and A. Piola (2005), On the relationship of satellite derived surface temperature fronts and chlorophyll-*a* in the western South Atlantic, *J. Geophys. Res.*, *110*, C11016, doi:10.1029/2004JC002736.

Saunders, P. M., and B. A. King (1995), Bottom currents derived from a shipborne ADCP on WOCE cruise A11, *J. Phys. Oceanogr.*, *25*, 329–347, doi:10.1175/1520-0485(1995)025<0329:BCDFAS>2.0.CO;2.

Smith, L. T., E. P. Chassignet, and D. B. Olson (1994), Wind-forced variations in the Brazil Malvinas Confluence region as simulated in a coarse-resolution numerical model of the South Atlantic, *J. Geophys. Res.*, *99*, 5095–5117, doi:10.1029/93JC03331.

Tansley, C. E., and D. P. Marshall (2001), On the dynamics of wind-driven circumpolar currents, *J. Phys. Oceanogr.*, *31*, 3258–3273, doi:10.1175/1520-0485(2001)031<3258:OTDOWD>2.0.CO;2.

Vigan, X., C. Provost, and G. Podesta (2000), Sea surface velocities from sea surface temperature image sequences: 2. Application to the Brazil-Malvinas Confluence, *J. Geophys. Res.*, *105*, 19,515–19,534.

Vivier, F., and C. Provost (1999a), Direct velocity measurements in the Malvinas Current, *J. Geophys. Res.*, *104*, 21,083–21,103, doi:10.1029/1999JC900163.

Vivier, F., and C. Provost (1999b), Volume transport of the Malvinas Current: Can the flow be monitored by TOPEX/Poseidon?, *J. Geophys. Res.*, *104*, 21,105–21,122, doi:10.1029/1999JC900056.

Vivier, F., C. Provost, and M. P. Meredith (2001), Remote and local forcing in the Brazil-Malvinas Region, *J. Phys. Oceanogr.*, *31*, 892–913, doi:10.1175/1520-0485(2001)031<0892:RALFIT>2.0.CO;2.

C. Provost and A. Spadone, LOCEAN, UMR7159, MNHN, IRD, Université Pierre et Marie Curie, CNRS, 4 place Jussieu, Tour 45-55, 5E, F-75252 Paris CEDEX 05, France. (aurelie.spadone@locean-ipsl.upmc.fr)